

Impacts of urbanization on air quality and related health risks in a city with complex terrain

Chenchao Zhan ^{a,b}, Min Xie ^{a,*}, Hua Lu ^{cb}, Bojun Liu ^{de}, Zheng Wu ^{cb}, Tijian Wang ^a, Bingliang Zhuang ^a, Mengmeng Li ^a, Shu Li ^a

^a School of Atmospheric Sciences, Nanjing University, Nanjing 210023, China

^b [School of Atmospheric Physics, Nanjing University of Information Science and Technology, Nanjing 210044, China](#)

^{cb} Chongqing Institute of Meteorological Sciences, Chongqing 401147, China

^{de} Chongqing Meteorological Observatory, Chongqing 401147, China

* Corresponding author. minxie@nju.edu.cn (M. Xie)–

Abstract: Urbanization affects air pollutants ~~viaby~~ urban expansion and emission growth, and thereby inevitably changes ~~the~~ health risks of air pollutants. However, the health risks related to urbanization are rarely estimated, especially for cities with complex terrain. In this study, a highly urbanized city with severe air pollution and complex terrain (Chengdu) is selected to explore this issue. The effects of urban expansion are further compared with emission growth ~~since as~~ air quality management ~~is usually achieved byis mainly to~~ regulating ~~anthropogenic~~ emissions. Air pollution in Chengdu ~~wasis~~ mainly caused by PM_{2.5} and O₃ ~~from 2015 to 2021~~. PM_{2.5} pollution tended ~~eds~~ to appear in cold months (November to February) ~~owingdue~~ to the ~~secondary circulation forced by~~ ~~complex terrain~~ ~~blocking of air~~ and the frequent temperature inversion, while O₃ pollution ~~wasis~~ likely to occur in warm months (April to August) because of high temperature and strong sunlight dominated by high-pressure systems. From 2015 to 2021, the ~~7-year~~ annual ~~average oftotal~~ premature mortalities from all non-accidental causes (ANAC) ~~dueattributed~~ to PM_{2.5} and O₃ ~~wereexposure are~~ ~~9386 (95%CI: 6542~11726)9386~~ and ~~8506 (95%CI: 4817~11882)7743~~, respectively. Based on the characteristics of PM_{2.5} and O₃, six numerical experiments ~~wereare~~ conducted to investigate the impacts of urban expansion and emission growth on health risks ~~of air~~ ~~pollutants~~. The results show that urban ~~land use~~ ~~expansion led to~~ ~~causes~~ an increase in air temperature and the boundary layer height, which ~~wasis~~ conducive to the diffusion of PM_{2.5}. Thus, ~~the monthly~~

average surface PM_{2.5} concentrations could decrease by 10.81.7 $\mu\text{g m}^{-3}$ (7.6%) in January. However, the monthly average daily maximum 8 h average (MDA8) O₃ concentrations could increase by 10.6 $\mu\text{g m}^{-3}$ (6.0%) in July owing due to the stronger photochemical production and better vertical mixing during ~~the~~ daytime. In this case ~~Correspondingly, the total~~ premature mortalities from ANAC ~~due~~ attributed to PM_{2.5} ~~exposure~~ decreased by 182-171 (95%CI: 129~200, or about 6.9%) (6.9%) in January, and but those ~~due~~ attributed to O₃ ~~exposure~~ increased by 203 (95%CI: 122~268, or about 9.5%) 203 (9.5%) in July. As for the effects of emission growth, the monthly average PM_{2.5} and MDA8 O₃ concentrations could ~~an~~ increase by 23.9 $\mu\text{g m}^{-3}$ (16.8%) 26.6 $\mu\text{g m}^{-3}$ and 4.8 $\mu\text{g m}^{-3}$ (2.7%) 4.8 $\mu\text{g m}^{-3}$ when anthropogenic emissions were ~~are~~ taken into account. ~~The total P~~ premature mortalities from ANAC ~~due~~ attributed to PM_{2.5} and O₃ ~~exposure~~ then increased by 388 (95%CI: 291~456, or about 15.7%) 424 (16.0%) and 87 (95%CI: 54~112, or about 4.1%) 87 (4.1%), respectively. From a health risk perspective, t ~~The effects~~ of urban land use ~~expansion~~ on health risks of PM_{2.5} are ~~is~~ about half that of anthropogenic emissions, and whereas the effects of urban land use ~~expansion~~ on health risks of O₃ can be 2-3 times that of anthropogenic emissions. This reminds us that, in addition to regulating anthropogenic emissions, urban planning ~~the development of cities~~ is also important for ~~the~~ urban air quality, especially for secondary pollutants like O₃, apart from the emissions reduction.

Key Words: urbanization; land use; anthropogenic emissions; air quality; health risk;

1 Introduction

Air pollutants are substances that damage humans, plants and animals drastically when present in the atmosphere in sufficient concentration (Baklanov et al., 2016; Kinney, 2018; Pautasso et al., 2010). The most common air pollutants found in air are ozone (O₃), fine particulate matter (PM_{2.5}, particulate matter with an aerodynamic diameter of 2.5 μm or less), sulfur dioxide (SO₂) and nitrogen oxides (NO_x, which is NO + NO₂). These air pollutants threaten human health in many parts of the world, evoking a series of health risks including cardiovascular diseases, respiratory diseases and chronic obstructive pulmonary disease (Brauer et al., 2016; Lelieveld et al., 2013; Manisalidis et al., 2020). According to the World Health Organization (WHO), exposure to ambient air pollutants is associated with ~~results in~~ 4.2 ~~about 4.2~~ million premature deaths annually globally

~~per year~~ (https://www.who.int/health-topics/air-pollution#tab=tab_2).

Most of those premature deaths occur in urban areas as urban areas currently host more than 50% of the population (over 3.5 billion people). ~~This proportion and this number~~ is projected to increase to 70% by 2050 ~~due to ongoing urbanization~~ (UNDESA, 2018)). ~~Urbanization since the industrial revolution in the 19th century has led to a profound modification of land use via urban expansion (Seto et al., 2012). Natural surfaces are replaced by impervious surfaces, then the surface physical properties (e.g., albedo, thermal inertia and roughness) and processes (e.g., the exchange of water, momentum and energy) are modified. These changes in surface physical properties and processes exert an important influence on urban meteorology and air quality, which has been widely acknowledged in previous studies. Wang et al. (2009) explored the impacts of urban expansion on weather conditions and its implication on O₃ concentration in the Pearl River Delta, and pointed out that urban land use changes can cause an increase in 2-m temperature by 1.0%~3.7%, an increase in planetary boundary layer height by 5.9%~6.3% and an increase in surface O₃ concentration by 4.2%~8.5%. Liao et al. (2015) conducted a similar study in the Yangtze River Delta, and found that urbanization increases 2-m temperature, planetary boundary layer and surface O₃ concentration but decreases surface PM₁₀ (particulate matter with an aerodynamic diameter of 10 μm or less) concentration. Similar conclusions about the impacts of urbanization on meteorology and air quality have also been reported in the Beijing-Tianjin-Hebei region (Yu et al., 2012) and the Sichuan Basin (Wang et al., 2021, 2022a).~~

What's more, urban areas are centers of resource utilization and are a major contributor to air pollutant and greenhouse gas emissions (Karl et al., 2019; Qian et al., 2022) and greenhouse gas emissions. According to the UN-Habitat (<https://unhabitat.org/topic/energy>), cities consume about 75% of global primary energy and emit 50%–60% of world greenhouse gas emissions, which is much more than in the past. Air pollution from these sources can sometimes accumulate and degrade urban air quality under unfavorable meteorological conditions characterized by weak winds, which leaves urban dwellers vulnerable to air pollution (Holman et al., 2015; Lin and Zhu, 2018). Excessive emissions are considered to be the root cause of poor air quality in urban areas, and the demand for urban air pollution control is increasing. Urbanization can increase urban land use and anthropogenic emissions, which will affect the concentrations as well as health risks of air pollutants. However, the health risks related to urbanization are rarely estimated, especially for those cities with complex terrain.

This is of great concern to policymakers and can inspire future air quality control strategies. —

Although building in the mountains is not as easy as in the plains — In addition to emissions, urban air quality is also closely related to meteorology (Qian et al., 2017; 2022). Under calm and clear weather conditions, local circulations mountain valley breezes driven induced by unequal heating and cooling of the valleys and mountains the thermal contrast of the topography, such as mountain valley breezes and sea land breezes, are likely to form and play an important role in air quality urban environment (Crosman and Horel, 2010; Zhan and Xie, 2022). Because of historical, political and economic reasons, about 12% of the global population (over 720 million people) resides in mountainous areas for historical, political, strategic and economic reasons. It is thus important to understand the fate of air pollutants in mountainous cities, where air pollution is usually more severe than in flat locations since mountainous terrain strongly alters the boundary layer structure, resulting in much more complicated diffusion conditions as the atmospheric dispersion is limited in mountainous areas (Zardi and Whiteman, 2013; Chow et al., 2013). The mountain-plain wind, resulting from horizontal temperature differences between air over mountain massifs and the air over the surrounding plains, is a key feature of the climatology of mountainous regions (Whiteman, 2000), which is important in determining the transport and dispersion of air pollutants. During daydurtime, the plain-to-mountain wind (plain wind) brings low-level air into the mountain massifs, whereas the mountain-to-plain wind (mountain wind) brings air out of the mountain massifs during nighttime. This wind system can often recirculate urban air pollutants and worsen air quality. Many notably pollution episodes appear in valley bottoms, along mountain slopes and in mountain basins. These include Examples can be found in examples like Mexico City (Molina et al., 2010), Hong Kong (Guo et al., 2013), the Seoul (Ryu et al., 2013), the Salt Lake Valley (Baasandorj et al., 2017), the Colorado Front Range (Bahreini et al., 2018), the Alps (Karl et al., 2019) and the Taiwan Island (Lee et al., 2019). Although the principles behind these examples apply to mountainous areas around the world, the phenomenon being described depends on the particular region (Whiteman, 2000; Oke et al., 2017). And a common principle is that diurnal wind systems driven by mountainous terrain can recirculate urban air pollutants and worsen air quality. —

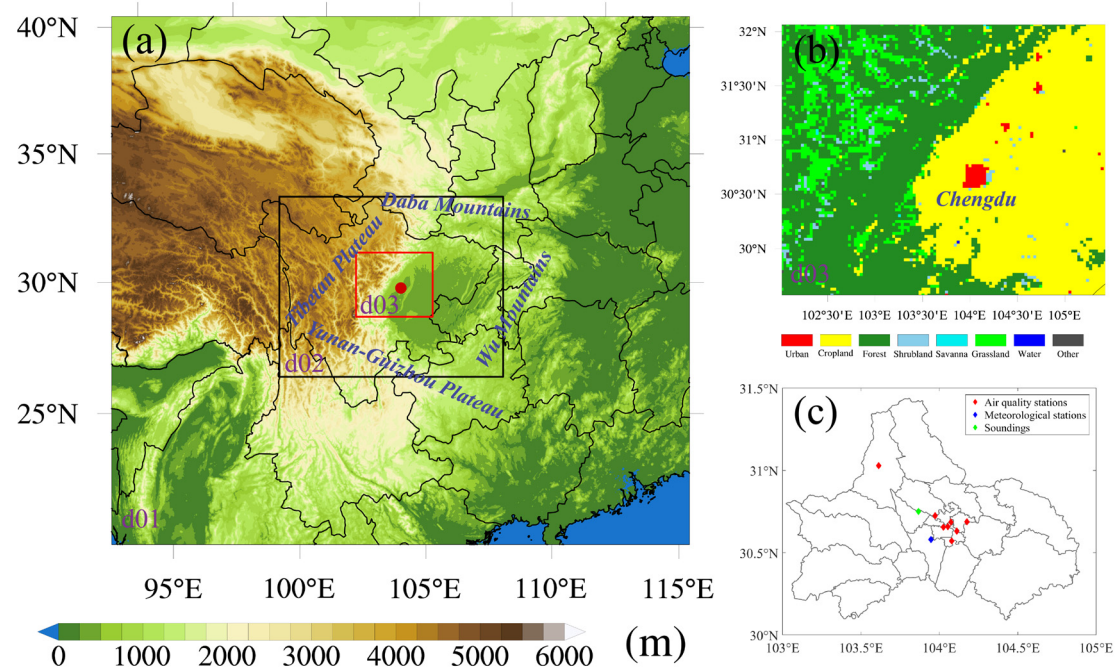
— The world has been undergoing urbanization since the industrial revolution in the 19th century (Seto et al., 2012), which directly leads to changes in land use via urban expansion. Natural

surfaces are replaced by impervious surfaces, then land surface physical properties (e.g., albedo, thermal inertia and roughness) and processes (e.g., the exchange of water, momentum and energy) are modified, hence altering the urban meteorology and air quality. This has been widely investigated using numerical models. For example, Liao et al. (2015) reported that urban expansion can cause an increase in 2-m temperature by 0.9–2.3 °C, a decrease in 10-m wind speed by 0.6–1.2 m s⁻¹ and an increase in planetary boundary layer height by 100–425 m in the Yangtze River Delta. These changes in meteorology further reduce surface PM₁₀ concentrations by 15.3–57.6 µg m⁻³ but increase O₃ concentrations by 1.7–8.3 ppbv. Changes in concentrations of air pollutants inevitably affect their health risks. However, the health risks related to urbanization are rarely estimated, especially for those cities with complex terrain. This is of great concern to policymakers and can inspire future air quality control strategies in mountainous areas.

—Chengdu (104.01°E, 30.70°N) is the largest city in western China, occupying an area of 12,390 square kilometers with a population of more than 20 million. Chengdu has the most complex terrain in the world. Located in the west of the Sichuan Basin, this city is surrounded by the Tibetan Plateau to the west, the Wu Mountains to the east, the Yunnan-Guizhou Plateau to the south and the Daba Mountains to the north (Figure 1a). In addition, the urbanization of Chengdu has developed rapidly Chengdu has experienced rapid urbanization over the past few decades with a surge in urban construction lands and a loss of cropland (Dai et al., 2021; Figure 1b). The fast urbanization process is generally accompanied by a surge in urban construction lands and the loss of cropland (Figure 1e). Luo et al. (2021) reported that Chengdu's urban area has increased by four times from 1996 to 2016. Due to Because of the substantial anthropogenic emissions from human activities —(Figure 1b)—and the poor atmospheric diffusion capacity caused by associated with complex terrain, Chengdu is one of the most polluted cities in China and has suffered from severe PM_{2.5} and O₃ pollution in recent years (Shu et al., 2021; Yang et al., 2020; Zhan et al., 2019). Complex terrain, rapid urbanization and severe air pollution make Chengdu an ideal place to study the impact of urbanization on health risks of air pollutants in mountainous areas. The results could also provide valuable insight for other cities with complex terrain in the world.

In this study, we systematically investigate evaluate the impacts of urbanization on air pollutants quality and the corresponding health risks in Chengdu. We also compare the impacts of

urban ~~expansion~~ ~~expansion~~ with ~~emission growth~~ ~~emission growth~~. First, the basic characteristics of air pollutants in Chengdu from 2015 to 2021 are ~~analyzed~~ ~~illustrated~~. Then, the impacts of urbanization on air pollutants are investigated ~~by~~ using the WRF-Chem model. Finally, premature mortalities attribut~~able~~ ~~ed~~ to changes in air pollutants are estimated ~~by~~ using the standard damage function. The rest of this paper is organized as follows. Section 2 introduces the ~~_~~ ~~observation~~ data, the model configurations and the experimental designs. Section 3 shows the main results and discussions. The conclusions are given in Section 4.



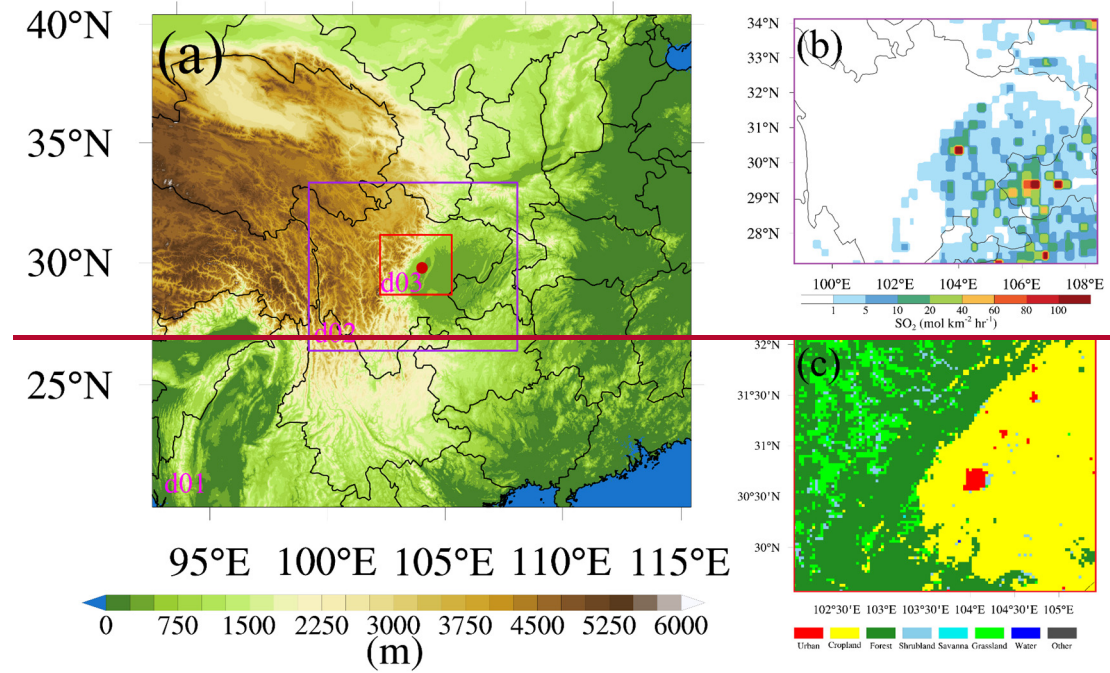


Figure 1. (a) Three-nested WRF-Chem Map of three nested WRF-Chem domains, including (a) domain 1 with terrain heights, (b) domain 2 with SO₂ emissions and (c) domain 3 with land cover maps and (c) locations of air quality stations, meteorological stations and soundings in Chengdu. The red dot in (a) shows the location of Chengdu.

2 Data Materials and methods

2.1 Air quality and meteorological Air pollutants and meteorological data

Air pollutants, including PM_{2.5}, PM₁₀, O₃, NO₂, SO₂ and CO, are monitored by the National Environmental Monitoring Center (NEMC) of China. These data are hourly issued on the national urban air quality real-time publishing platform (<http://106.37.208.233:20035/>). The monitoring data are strictly in accordance with the national monitoring regulations (<http://www.cnemc.cn/jcgf/dqhj/>). It should be noted that the O₃ measurements are reported in the unit of $\mu\text{g m}^{-3}$ at the standard atmospheric conditions (273.15 K, 1 atm) before September 2018, and at 298.15 K conditions afterward. There are eight air quality stations throughout Chengdu (Figure 1c), and the urban hourly pollutants are the average results of measurements at all monitoring sites. The daily PM_{2.5} concentrations are obtained by averaging observations over 24 hours of the day. The daily maximum 8 h average (MDA8) O₃ concentrations are calculated only on days with more than 18 h of O₃ measurements. This nationwide observation network consists of more than 2300 stations distributed

~~over 450 cities in China.~~

Surface meteorological data, including 2-m air temperature (T_2), ~~relative humidity (RH)~~2-m dew point temperature (TD_2), ~~and~~ 10-m wind speed (WS_{10}) and 10-m direction (WD_{10}), are taken from the website of the University of Wyoming at station ZUUU (<http://weather.uwyo.edu/surface/>). To verify upper-air fields, the sounding observations at Wenjiang (~~103.87°E, 30.75°N~~station 56187) ~~in Chengdu~~ are also acquired from this website. These sounding data contain temperature, dew point temperature ~~relative humidity~~ and wind speed, etc. at different pressure layers with a time resolution of 12 h (00:00 and 12:00 UTC), and are often plotted on a Skew-T diagram (<https://www.ncl.ucar.edu/Applications/skewt.shtml#ex2>).

~~— In this study, the data quality control are performed as follows. First, the data indicated as missing are set as invalid. Second, the urban values are calculated by averaging observations at all monitoring sites in Chengdu. Third, the daily maximum 8 h average (MDA8) O_3 concentrations are calculated only on days with more than 18 h of O_3 concentrations measurements.—~~

2.2 WRF-Chem model and experimental designs

WRF-Chem is the Weather Research and Forecasting (WRF) model coupled with Chemistry, in which meteorological and chemical variables use the same coordinates, transport schemes and physics schemes in space and time (Grell et al., 2005). WRF-Chem version 3.9.1 is employed in this study. As shown in Figure 1a, three nested domains are used with the grid spacing of 27, 9 and 3 km, respectively. 32 sigma levels are extending from the surface to 100 hPa in the vertical direction with 12 levels located below 2 km to resolve the boundary layer processes. The size of the lowest vertical grid is about 25 m. The MODIS-based land use data set as default in WRF are selected. The domains and main options for physical and chemical parameterization schemes are listed in Table 1. The National Centers for Environmental Prediction (NCEP) ~~global final~~Final (FNL) reanalysis data with a ~~horizontal~~ resolution of $1^\circ \times 1^\circ$ at 6 h time intervals are adopted as the initial and boundary conditions for meteorological fields. Anthropogenic emissions are provided by the Multi-resolution Emission Inventory for China (MEIC) ~~in 2017~~ with a grid resolution of $0.25^\circ \times 0.25^\circ$ ~~resolution~~. Biogenic emissions are calculated online using the Guenther scheme (Guenther et al., 2006).

Table 1. The domains and main options for WRF-Chem.

Items	Contents
Domains (x, y)	(94, 86), (109, 88), (112, 94)
Grid spacing (km)	27, 9, 3
Center	(104°E, 31°N)
Time step (s)	90
Microphysics	Purdue Lin scheme (Chen and Sun, 2002)
Longwave radiation	RRTM scheme (Mlawer et al., 1997)
Shortwave radiation	Goddard shortwave scheme (Matsui et al., 2018)
Surface layer	Monin-Obukhov scheme (Janjic, 1994)
Land-surface layer	Unified Noah land-surface model (Tewari et al., 2014)
Planetary boundary layer	Mellor-Yamada-Janjic TKE scheme (Janjic, 1994)
Cumulus parameterization	Grell 3D ensemble scheme (Grell and Devenyi, 2002)
Gas-phase chemistry	RADM2 (Stockwell et al., 1990)
Photolysis scheme	Fast-J photolysis (Fast et al., 2006)
Aerosol module	MADE/SORGAM (Schell et al., 2001)

208

209 To ~~estimate~~investigate the impacts of ~~urban expansion and anthropogenic~~
210 ~~emissions~~urbanization, six numerical ~~simulation~~experiments are designed (Table 2). The year of
211 the numerical simulations is 2017 since the ~~MEIC emission inventory~~anthropogenic emissions ~~is~~are
212 currently updated to 2017. ~~Taking into account the computational cost~~Moreover, January is ~~the~~
213 representative of the cold months with frequent PM_{2.5} pollution, while July ~~is the~~ representative ofs
214 the ~~warm months~~hot season with frequent O₃ pollution (Section 3.1). Jan_Base~~simulation~~ is a
215 baseline simulation using the MODIS land use~~—~~and the MEIC~~anthropogenic~~ emission inventory
216 over all three domains. ~~The~~SO₂ emissions in domain 2 and land cover maps in domain 3 are
217 ~~particularly illustrated shown~~ in Figure ~~1b, 1c and 1e~~. Jan_noCD is a sensitivity simulation, in which
218 the urban land ~~uses~~surface of Chengdu is replaced by cropland to examine the impacts of urban
219 ~~expansion~~expansion. Jan_noEmi is ~~another~~also a sensitivity simulation, in which the anthropogenic
220 emissions in Chengdu are shut down to identify the impacts of ~~emission growth~~anthropogenic
221 ~~emissions~~. The above three numerical experiments used the same configurations (Table 1) running

from 00:00 UTC December 28, 2016 to 00:00 UTC February 1, 2017 with the first 96 h as spin-up time. July_Base, July_noCD and July_noEmi are the same as Jan_Base, Jan_noCD and Jan_noEmi, but run from 00:00 UTC June 27 to 00:00 UTC August 1, 2017 with the first 96 h as spin-up time.

Table 2. Six numerical ~~experiments~~ simulations are conducted in this study.

Scenarios	Description
Jan_Base	Baseline simulation in January
Jan_noCD	Replacing urban land use of Chengdu with cropland in January
Jan_noEmi	Shutting down anthropogenic emissions in Chengdu in January
July_Base	Baseline simulation in July
July_noCD	Replacing urban land use of Chengdu with cropland in July
July_noEmi	Shutting down anthropogenic emissions in Chengdu in July

2.3 Health risks estimation

Daily premature mortalities attributed to $\text{PM}_{2.5}$ and O_3 exposure from all non-accidental causes (ANAC), cardiovascular diseases (CVD), respiratory diseases (RD) and chronic obstructive pulmonary diseases (COPD) are estimated using the standard damage function (Anenberg et al., 2010; Zhan et al., 2021):

$$\Delta M = y_0 \left(\frac{RR - 1}{RR} \right) \text{Pop}, \quad (4)$$

where ΔM is the daily premature mortality, y_0 is the daily baseline mortality rate, RR is the relative risk, $(RR-1)/RR$ is the attributable fraction, and Pop is the exposed population. RR is calculated as follows:

$$RR = \exp(\beta(C - C_0)), \quad (5)$$

where β is the concentration-response function that relates a unit change in air pollutant concentrations to a change in health endpoint incidence~~concentration-response function~~. In practice, β represents the percent change of mortality per $10 \mu\text{g m}^{-3}$ increase of daily $\text{PM}_{2.5}$ /MDA8 O_3 concentration with 95% confidence intervals (95% CI), ~~which represents the percentage increase in health effect per $1 \mu\text{g m}^{-3}$ $\text{PM}_{2.5}$ and MDA8 O_3 increment~~. C is the exposure concentration, which is the daily average concentration for $\text{PM}_{2.5}$ and the MDA8 O_3 concentration for O_3 , and C_0 is the

threshold concentration. When C is not greater than C₀, the value of C-C₀ is 0.

In this study, C₀ ~~for PM_{2.5}~~ is 10 µg m⁻³ for daily PM_{2.5} (Song et al., 2015), ~~and, and _ for MDA8 O₃ is 75.2 µg m⁻³ for MDA8 O₃~~ (Liu et al., 2018). ~~The~~ β and y₀ ~~values~~ for ANAC, CVD, RD and COPD are summarized in Table 3 (Chen et al., 2017; Yin et al., 2017). The populations of Chengdu provided by the National Bureau of Statistics of China are 16.853 million, 18.582 million, 19.188 million, 19.183 million, 20.409 million, 20.947 million and 20.938 million from 2015 to 2021.–

We first calculate the PM_{2.5}- and O₃-induced daily premature mortalities using the methods mentioned above, and then add up the daily premature mortalities for the whole year/month to get the total premature mortalities. Since the largest uncertainty among the factors that determine premature mortalities usually comes from β, premature mortalities are presented as means and 95% CI based on β at 95% CI in this study. In addition, it should be noted that we use the average of air pollutant concentration at all monitoring sites to represent air pollutant concentration in Chengdu. Correspondingly, the total population of Chengdu is used as the exposed population. So our results are for Chengdu as a whole and do not address the spatial distribution of premature mortalities.

Table 3. Daily β (95%CI) and y₀ values for ANAC, CVD, RD and COPD. ~~This table is cited from Wang et al. (2021).–~~

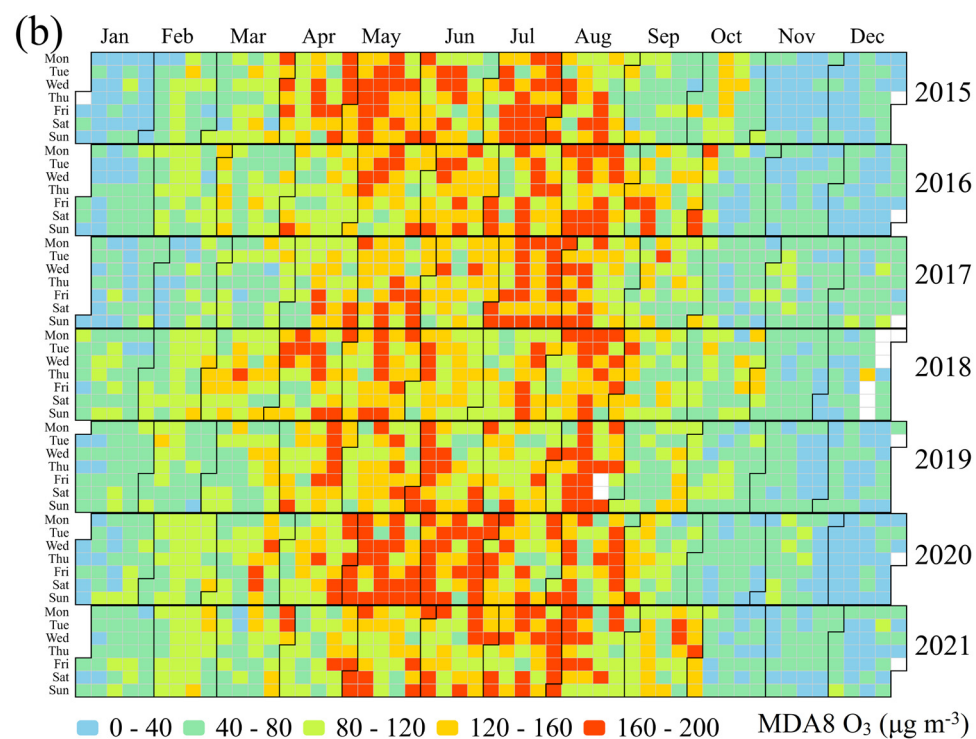
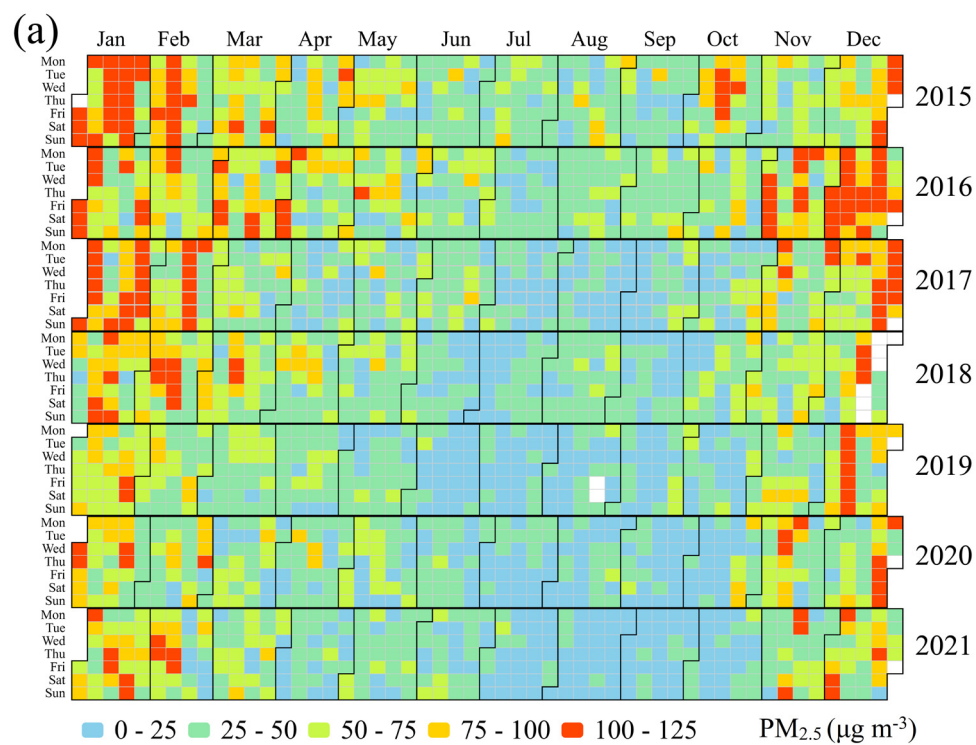
Disease	β for PM _{2.5} (%)	β for MDA8 O ₃ (%)	y ₀
ANAC	0.22 <u>(0.15, 0.28)</u>	0.24 <u>(0.13, 0.35)</u>	1.687×10 ⁻⁵
CVD	0.27 <u>(0.18, 0.36)</u>	0.27 <u>(0.10, 0.44)</u>	3.880×10 ⁻⁶
RD	0.29 <u>(0.17, 0.42)</u>	0.18 <u>(-0.11, 0.47)</u>	1.841×10 ⁻⁶
COPD	0.38 <u>(0.23, 0.53)</u>	0.20 <u>(-0.13, 0.53)</u>	1.623×10 ⁻⁶

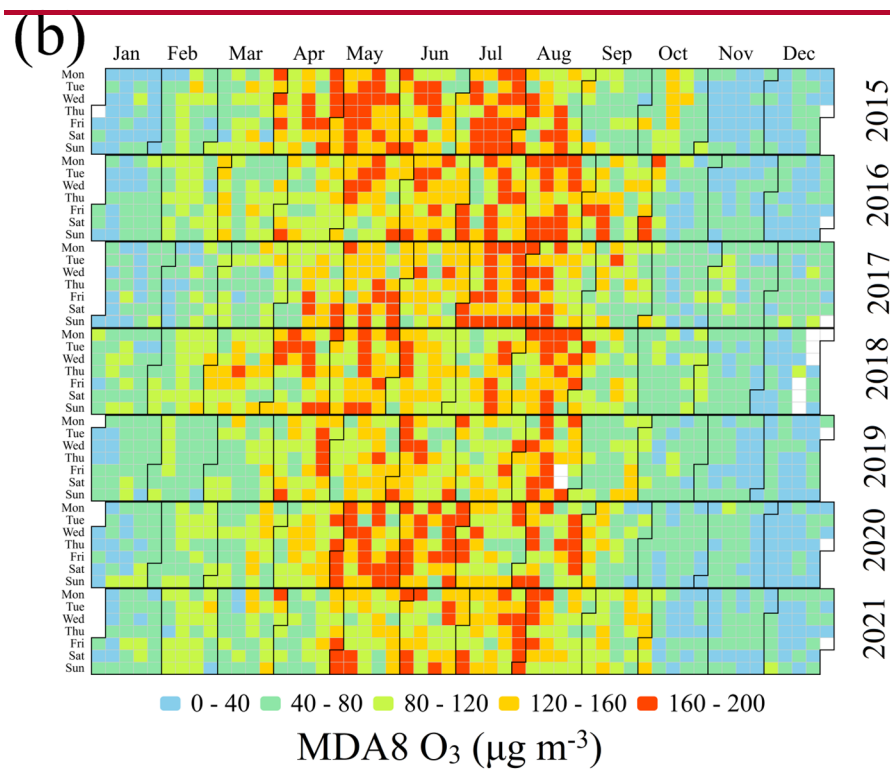
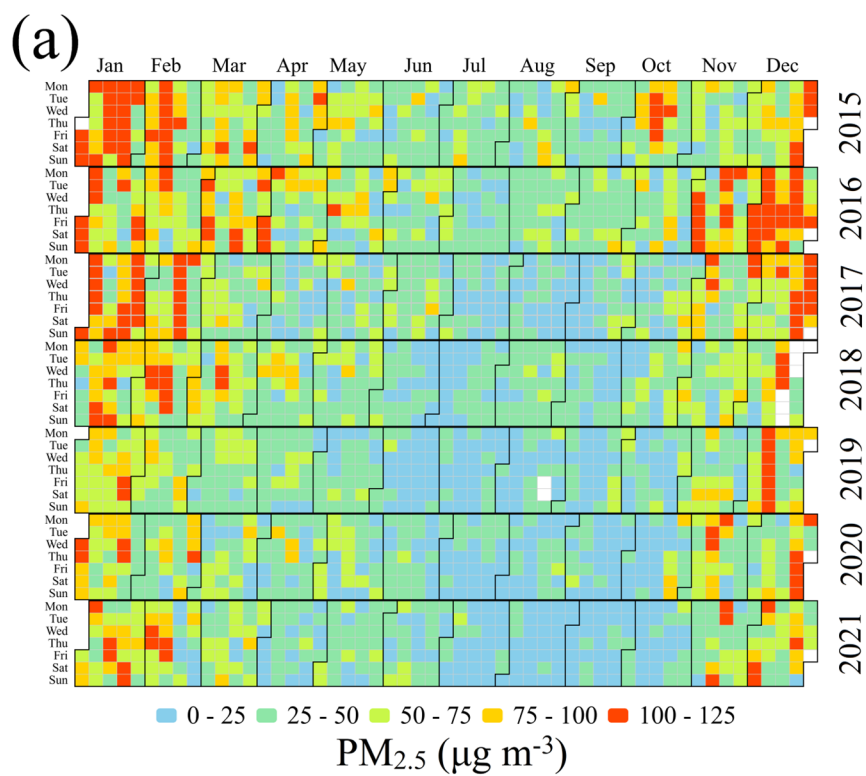
3 Results and discussions

3.1 PM_{2.5} and O₃ pollution in Chengdu

PM_{2.5} and O₃ are two crucial air pollutants According to Chinese ambient air quality standards, PM_{2.5} pollution occurs when daily PM_{2.5} concentrations are greater than 75 µg m⁻³, and O₃ pollution occurs when MDA8 O₃ concentrations are greater than 160 µg m⁻³ ~~that account for air pollution~~. As shown in Figure 2, Chengdu is suffering from severe PM_{2.5} and O₃ pollution in recent years. The

Chinese ambient air quality standards for PM_{2.5} and MDA8 O₃ are 75 µg m⁻³ and 160 µg m⁻³, respectively. As shown in Figure 2, Chengdu is suffering from severe PM_{2.5} and O₃ pollution in recent years. There were 97, 101, 68, 53, 33, 43 and 37 PM_{2.5} pollution episodes, and 61, 48, 42, 40, 42, 71 and 48 O₃ pollution episodes in Chengdu from 2015 to 2021. In China, the annual evaluation criterion for PM_{2.5} is the annual average concentration, and it for O₃ is the 90th percentile of MDA8 O₃ concentration. The annual average concentrations of PM_{2.5} were 60.7, 59.9, 52.6, 47.2, 40.6, 40.8 and 40.1 µg m⁻³, and those of the 90th percentile of MDA8 O₃ concentrations were 183.095.3, 167.096.4, 168.095.8, 164.0401.3, 171.586.8, 188.992.0 and 167.189.6 µg m⁻³ in Chengdu from 2015 to 2021, respectively. This suggests that in terms of the annual average concentrations, PM_{2.5} pollution had improved significantly while O₃ pollution had not. O₃ pollution control in Chengdu should be taken seriously in the future. In addition, PM_{2.5} and O₃ pollution have had clear seasonal preferences, that is, PM_{2.5} pollution tended to appear in cold months (November to February) while O₃ pollution preferred to appear in warm months (April to August). High PM_{2.5} concentrations in cold months may be associated with the consumption of fossil fuels for heating and frequent temperature inversion. The high temperature and strong sunlight contribute to the elevated O₃ concentrations in warm months. Elevated O₃ concentrations in warm months are contributed to the high temperature and strong sunlight.





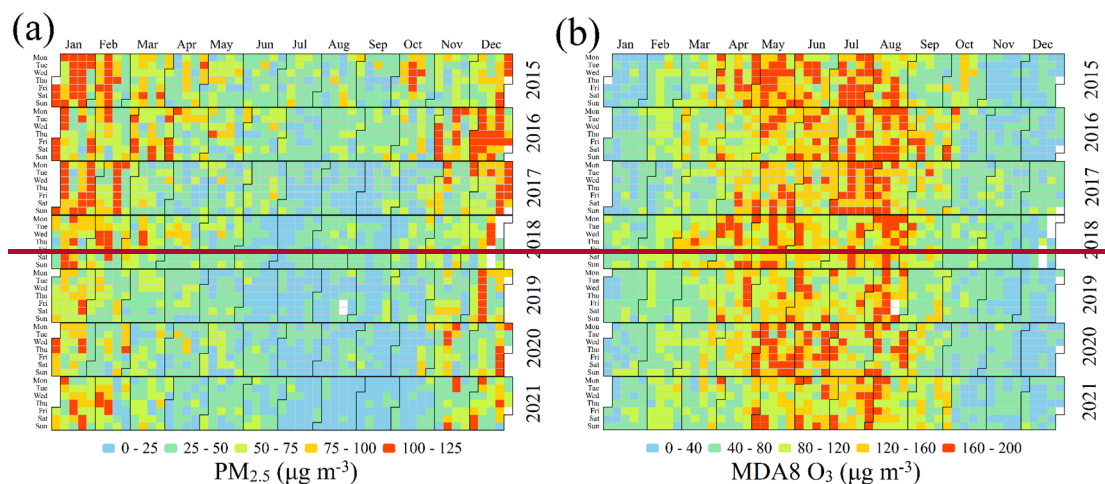


Figure 2. Heat maps of Distribution of (a) daily-average PM_{2.5} and (b) MDA8 O₃ concentrations in Chengdu from 2015 to 2021.

3.2 Premature mortality attributable to PM_{2.5} and O₃

Severe PM_{2.5} and O₃ pollution are responsible for a considerable-large number of premature mortalities in Chengdu. From 2015 to 2021, As shown in Table 4, the premature mortalities from ANAC due attributed to PM_{2.5} were exposure are 10596 (95%CI: 7420~13186), 11647 (95%CI: 8140~14518), 10154 (95%CI: 7116~12630), 8942 (95%CI: 6214~11198), 7992 (95%CI: 5540~10031)3, 8298 (95%CI: 5759~10402) and 8072 (95%CI: 5606~10115) from 2015 to 2021, with the 7-year annual average of 9386 (95%CI: 6542~11726). The highest health risk among the diseases was from CVD with a 7-year annual average of 2609 (95%CI: 1788~3384), followed by COPD with a 7-year annual average of 1485 (95%CI: 941~1983) and RD with a 7-year annual average of 1321 (95%CI: 804~1840). This was mainly associated with the daily baseline mortality rate of different diseases (Table 3). Due to urbanization and administrative division adjustment, Although Chengdu's population has been increases by 24.2% by 24.2% from 2015 (16.853 million) to 2021 (20.938 million), In contrast, the total premature mortalities attributed to due to PM_{2.5} have generally declined (Figure 3a) falls by 23.8% from 2015 (10596) to 2021 (8072). The reduction in premature mortalities is mainly contributed to the reduction in PM_{2.5} concentrations since the annual average PM_{2.5} concentrations decrease from 60.7 µg m⁻³ in 2015 to 40.1 µg m⁻³ in 2021 (Section 3.1), suggesting that air pollution control can bring huge health benefits owing to reduced PM_{2.5} concentrations in recent years (Section 3.1).

Unlike the overall reduction in premature mortalities due to PM_{2.5}, the premature mortalities

due to O₃ fluctuate. The premature mortalities from ANAC attributed to O₃ exposure are due to O₃ were 7657 (95%CI: 4345~10672), 8025 (95%CI: 4537~11227), 7870 (95%CI: 4451~11005), 8824 (95%CI: 4967~12397)8556, 7919 (95%CI: 4483~11065)6367, 10085 (95%CI: 5749~13999)8300 and 9163 (95%CI: 5185~12809)7429 from 2015 to 2021, with a 7-year annual average of 8506 (95%CI: 4817~11882)7743, about 980% of that due attributed to PM_{2.5} exposure. The total premature mortalities attributed to O₃ exposure in 2021 (7429) are only 3.0% lower than that in 2015 (7657). This is in line with the insignificant reduction of O₃ concentrations in Chengdu from 2015 to 2021, indicating that O₃ pollution control in Chengdu still has great potential and significance. Unlike the overall reduction in premature mortalities due to PM_{2.5}, the premature mortalities due to O₃ increased slightly (Figure 3a), further indicating the urgent need for powerful O₃ control strategies in Chengdu.

Table 4. Premature mortality from ANAC, CVD, RD and COPD attributed to PM_{2.5} and O₃ exposure.

Year	PM _{2.5}				MDA8-O ₃			
	ANAC	CVD	RD	COPD	ANAC	CVD	RD	COPD
2015	10596	2935	1485	1660	7657	1957	643	624
2016	11647	3231	1635	1832	8025	2053	672	653
2017	10154	2812	1422	1589	7870	2013	659	641
2018	8942	2490	1262	1424	8556	2191	715	696
2019	7993	2230	1131	1280	6367	1630	532	518
2020	8298	2313	1173	1325	8300	2121	696	677
2021	8072	2249	1140	1287	7429	1902	621	604

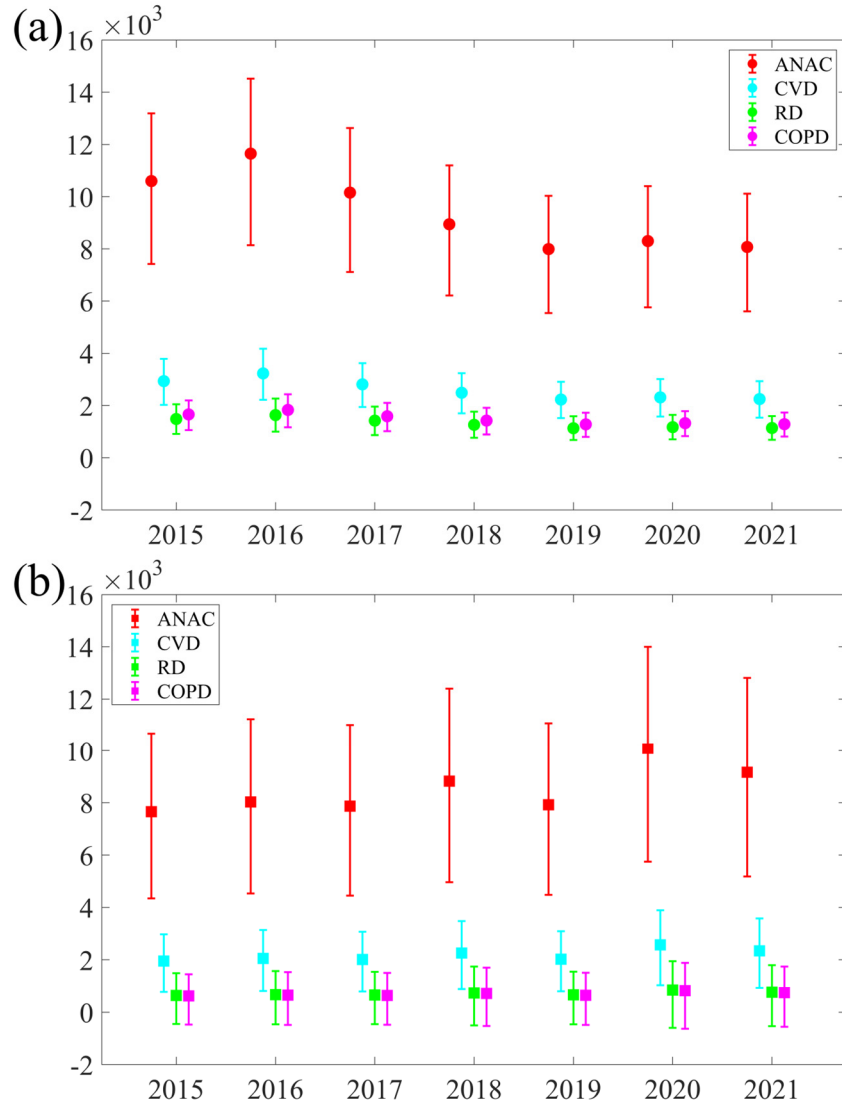


Figure 3. Premature mortality from ANA, CVD, RD and COPD attributable to $PM_{2.5}$ and O_3 in Chengdu from 2015 to 2021.

3.3 Impacts of urbanization on $PM_{2.5}$ and O_3

3.3.1 Meteorological conditions in January and July

In this study, January and July 2017, when $PM_{2.5}$ and O_3 pollution episodes are likely to occur (Figure 2), are chosen selected for simulations to study the role of urbanization and analysis when $PM_{2.5}$ and O_3 pollution are likely to occur (Figure 2). In January 2017, Chengdu experienced $PM_{2.5}$ pollution for 23 out of 31 days with a monthly an average concentration of $128.85 \mu g m^{-3}$. From the perspective of atmospheric circulations, westerly winds prevailed ed over Chengdu due to the large north-south geopotential height gradient at 500 hPa (Figure 43a). However, the cold westerly winds

were from the north are blocked by the Tibetan Plateau and thereby the elimination of PM_{2.5} was limited. Instead At 700 hPa, a low-pressure system, called the Southwest Vortex, appears to the left of the southwestern air flow originating from the Bay of Bengal could reach Chengdu (Figure 4b Chengdu at 850 hPa (Figure 3b). Warm and humid southerly air flows can reach Chengdu affected by this low-pressure system. This warm advection was conducive to the formation of an inverse layer near 700 hPa (Figure 4c and d), which made the vertical diffusion of PM_{2.5} difficult. Hu et al., 2021; Ning et al., 2018). The dry air in the upper layer and moist air in the lower layer lead to a strong temperature inversion appearing from 700 hPa to 500 hPa (Figure 4a and b). The blocking of cold air and the temperature inversion make PM_{2.5} pollution frequent during this period. were two important reasons for frequent PM_{2.5} pollution episodes during this period (Hu et al., 2021; Ning et al., 2018).

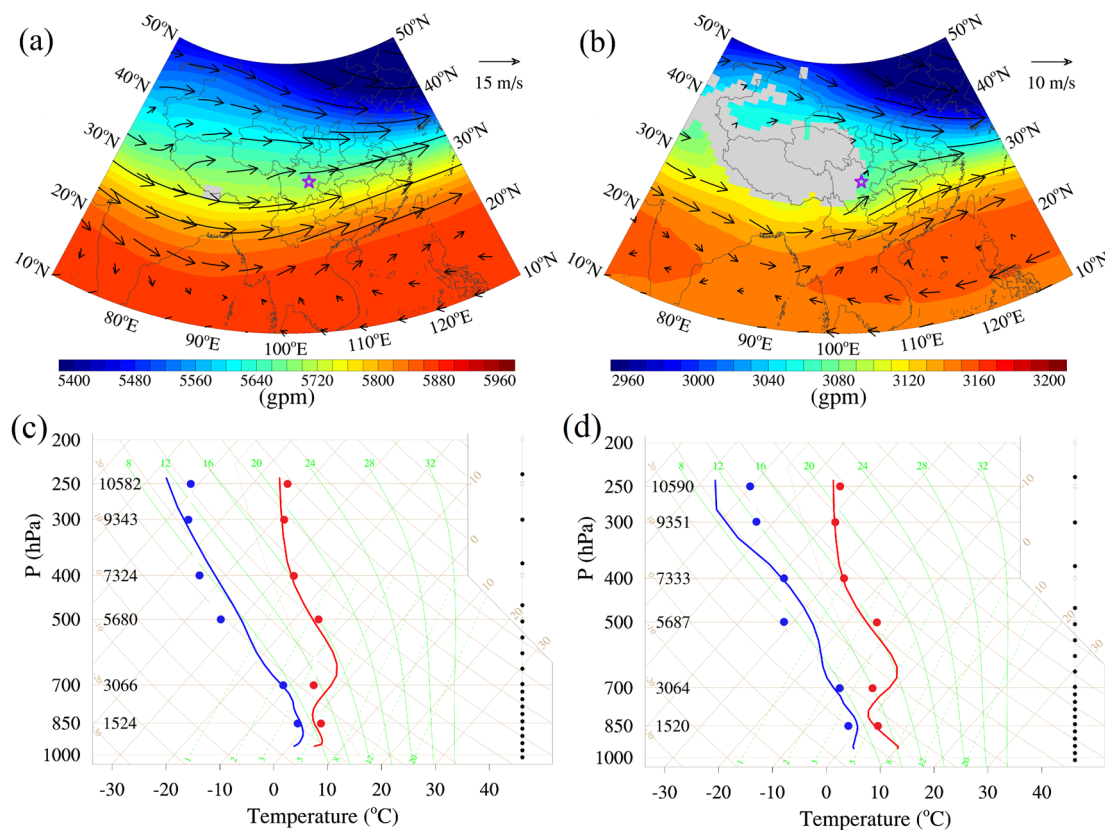


Figure 4. The weather charts at (a) 500 hPa and (b) 700 hPa for January 2017 are based on the NCEP FNL reanalysis data. The purple pentacles show the location of Chengdu. The skew-T diagram at (c) 00:00 UTC and (d) 12:00 UTC in January 2017. The red and blue lines are the simulated air temperature and dew point temperature in Jan Base simulation, while the

red and blue points are the sounding temperature and dew point temperature. These results are monthly averages.

In July 2017, there ~~were~~ 19 days of O₃ pollution in Chengdu, and the monthly average MDA8 O₃ concentration ~~was~~ 172.9 $\mu\text{g m}^{-3}$. At 500 hPa, Chengdu ~~was~~ dominated by strong high-pressure systems, and thereby air temperature ~~was~~ high and wind speed ~~was~~ small (Figure ~~53ea~~). The monthly average T₂ ~~was~~ as high as 28.6 °C while the monthly average WS₁₀ ~~was~~ only 1.6 m s⁻¹ during this period (Figure 5b)in July. These meteorological conditions are conducive to the formation of O₃ pollution. High temperature favored photochemical reactions of O₃ while weak winds trapped O₃. Furthermore, the frequency and thickness of temperature inversion in July ~~were~~ far less than those in January (Figure ~~4c and d; Figure 5c and d4~~). Well-developed boundary layer facilitated vertical mixing of Then O₃ ~~can be well mixed~~ within the boundary layer ~~mixing layer~~ during the daytime, which is an important way to maintain high surface O₃ concentrations during the daytime (Aneja et al., 2000; Tang et al., 2017).

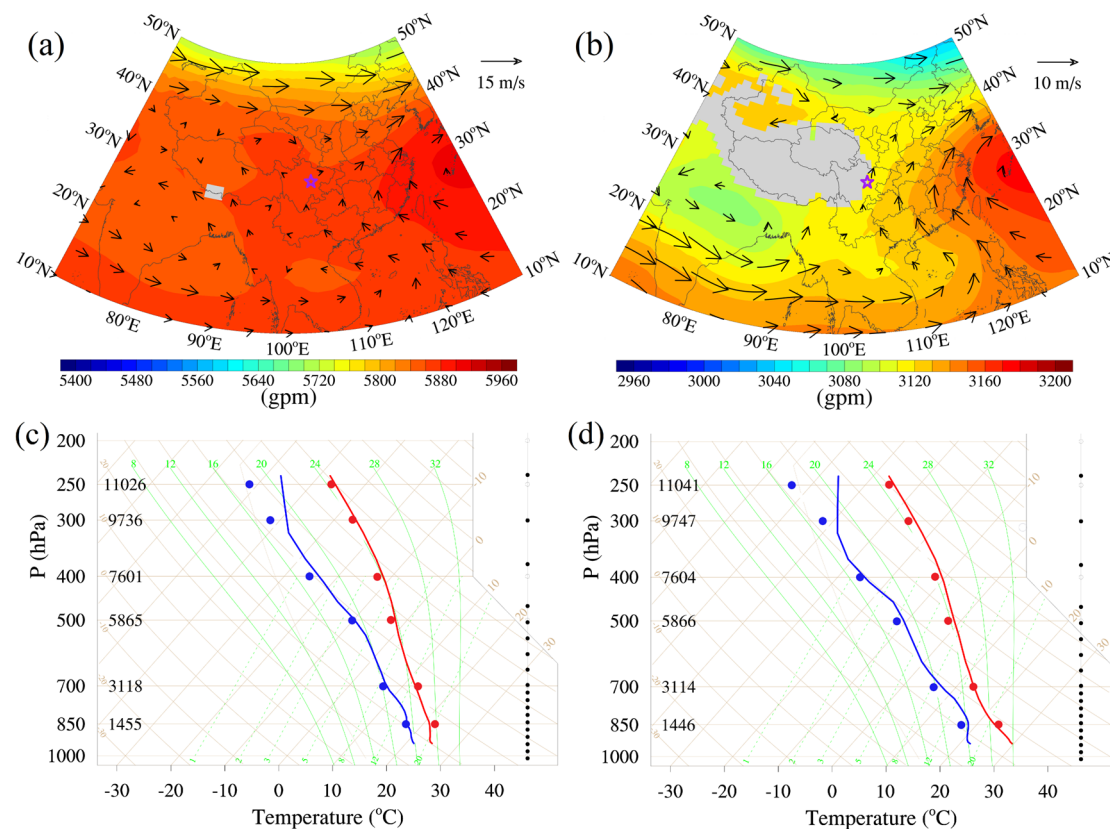


Figure 5. The weather charts at (a) 500 hPa and (b) 700 hPa for July 2017 are based on the NCEP FNL reanalysis data. The purple pentacles show the location of Chengdu. The skew-T diagram at (c) 00:00 UTC and (d) 12:00 UTC in July 2017. The red and blue lines are the simulated air temperature and dew point temperature in July Base simulation, while the red and blue points are the sounding temperature and dew point temperature. These results are monthly averages.

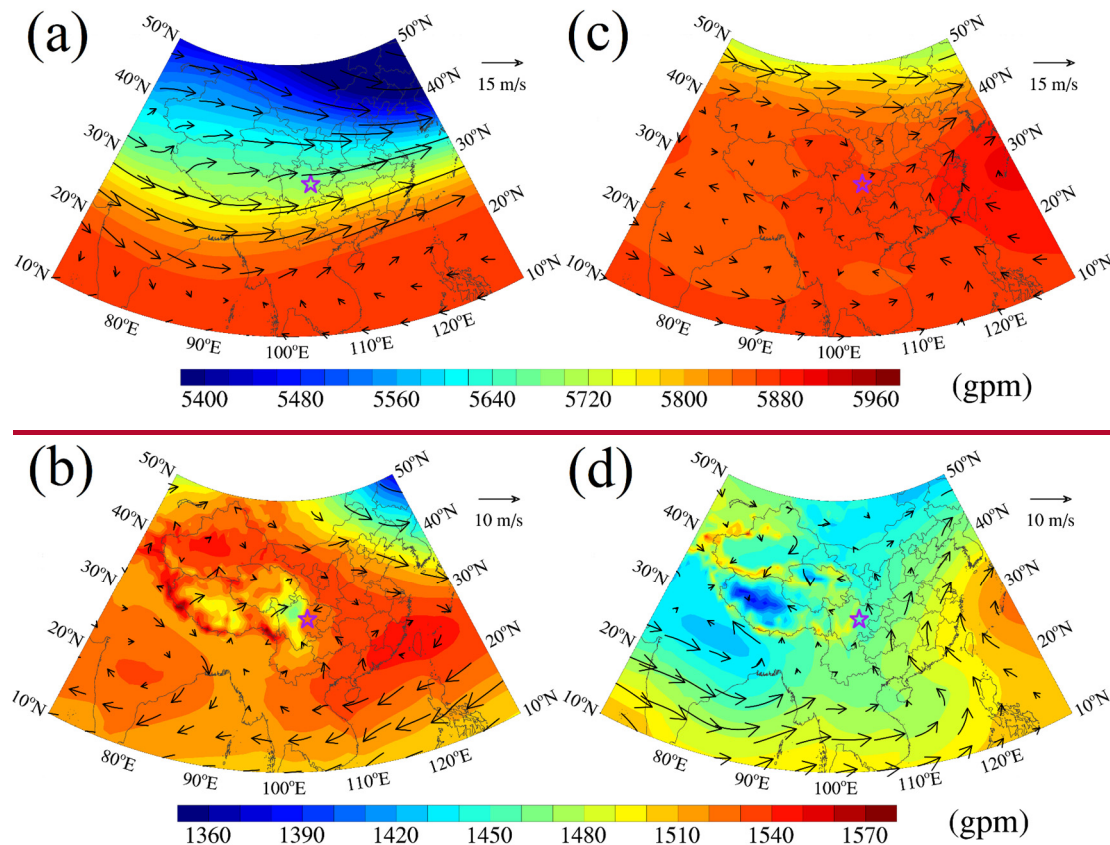
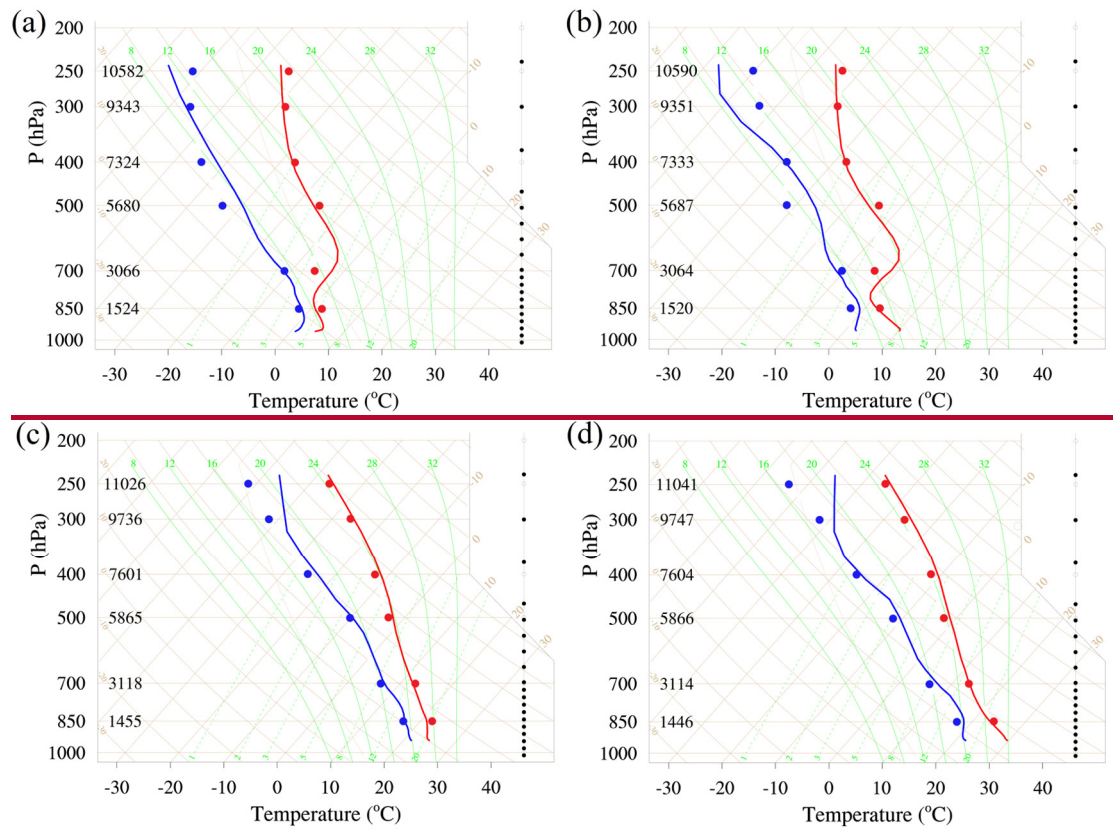


Figure 3. The weather charts at (a) 500 hPa and (b) 850 hPa for January 2017. (c) and (d) are the same as (a) and (b), but for July 2017. The purple pentacles show the location of Chengdu. These weather charts are based on the NCEP global final analysis data.—



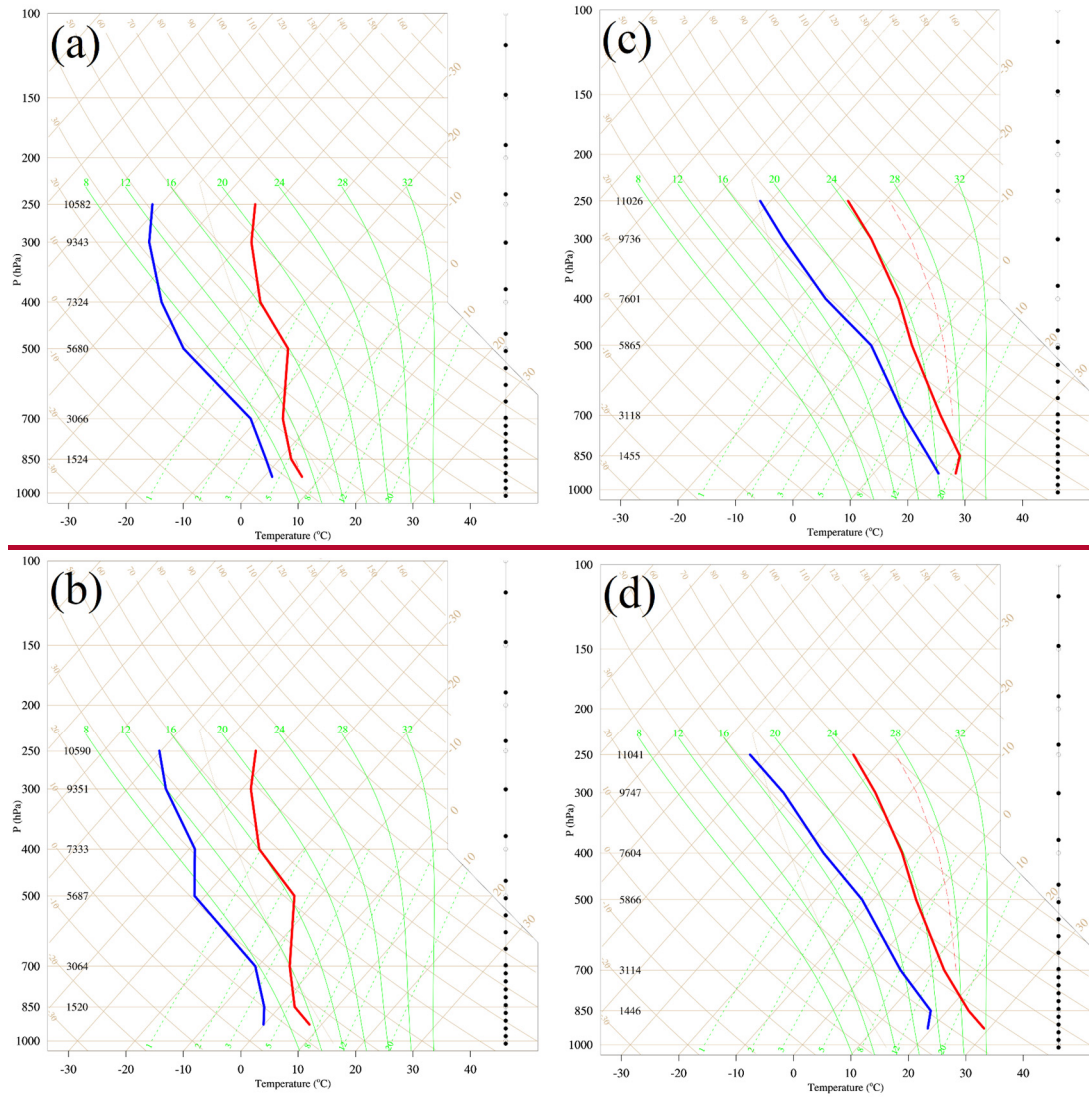
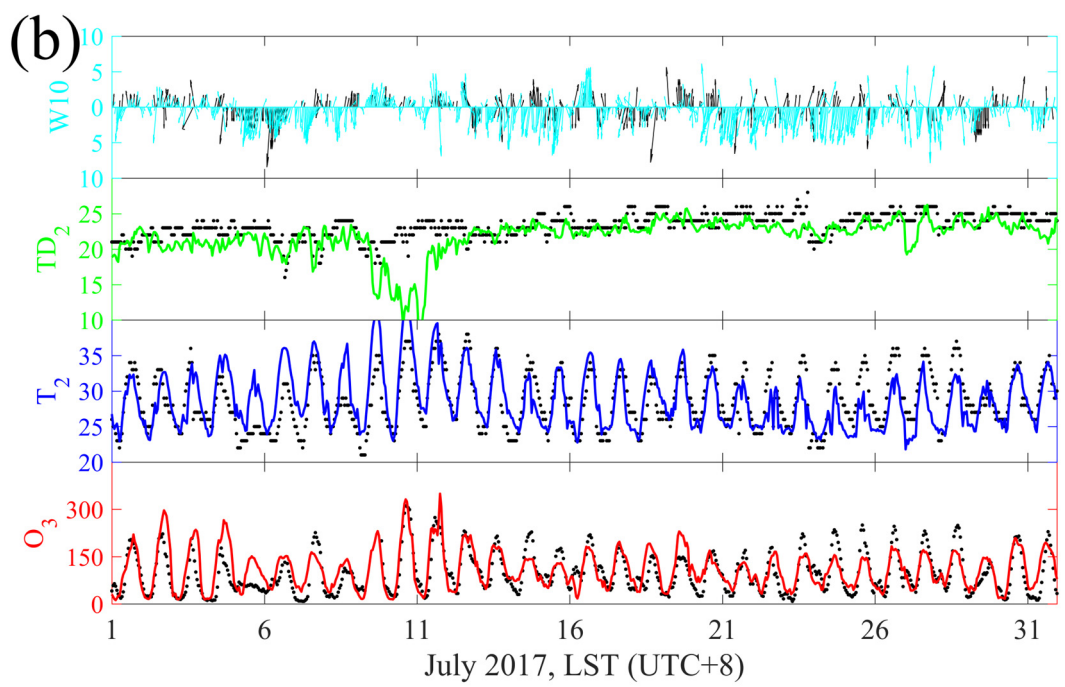
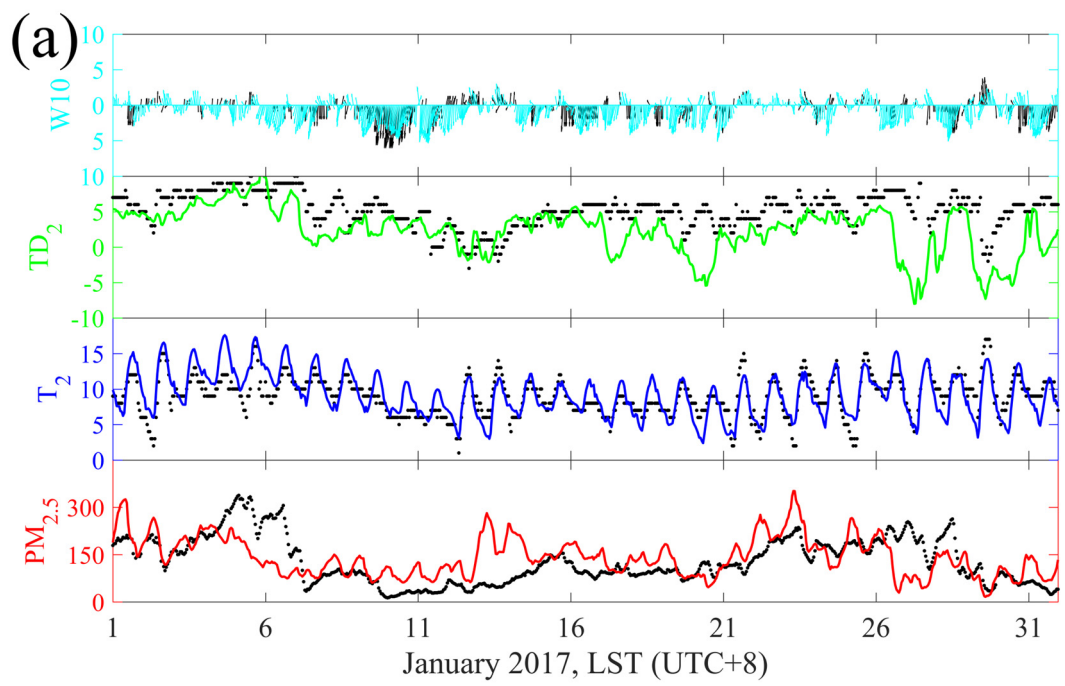


Figure 4. The skew-T diagram at (a) 00:00 UTC and (b) 12:00 UTC in January 2017. (c) and (d) are the same as (a) and (b), but for July 2017. The red and blue lines indicate air temperature and dew point temperature, respectively. The red and blue points are the sounding temperature and dew point temperature.

3.3.2 Evaluation of model performance

We first compare vertical profiles in the model with the sounding data to determine whether the model captures the vertical structure of the tropospheric atmosphere. As shown in Figure 4c-d and 5c-d, the WRF-Chem model can successfully simulate the changes in temperature and dew point temperature in the vertical direction, whether in January or July, day or night. Therefore, the vertical results in the model are reliable. Furthermore, simulations at the lowest model level are

compared with surface observations, and the results are presented in Figure 6. The mean bias (MB) of the simulated and observed concentrations of Simulated $\text{PM}_{2.5}$ concentrations, O_3 concentrations, air temperature, relative humidity and wind speed in baseline simulations are compared with the observations to verify the model performance (Figure 5). The magnitudes of simulated $\text{PM}_{2.5}$ and O_3 are reasonable with the small mean bias (MB) of $12.723.4 \mu\text{g m}^{-3}$ and $11.6 \mu\text{g m}^{-3}$, with the normalized mean bias (NMB) values of 9.9% and 12.0%, which are within the acceptable standards ($\text{NMB} < \pm 15\%$) respectively. The high correlation coefficients (COR) for $\text{PM}_{2.5}$ (0.44) and O_3 (0.77) indicate that simulations reproduce well the diurnal variation in pollutants are 0.44 and 0.77, respectively. The statistical metrics for $\text{PM}_{2.5}$ and O_3 are similar to those in previous studies (Wang et al., 2022b; Wu et al., 2022), indicating that Therefore, our the modeling results for $\text{PM}_{2.5}$ and O_3 are generally reasonable and acceptable. With regard to the meteorological factors, T_2 is well simulated with low MB (0.2 and 0.1 °C) and high COR (0.76 and 0.70) values in both January and July. The simulations Our simulation underestimates TD_2RH to some extent with (the MB values are -14.3% -1.5°C and -2.6°C -4.8% in January and July, respectively), but the diurnal variation of RH is well represented (the COR values are 0.54 and 0.64). As for 10-m wind WS_{10} , poor simulation results are predictable in the case of low wind and complex terrain. The WS_{10} in the model is overestimated (the MB values are 1.3 and 1.7 m s^{-1}) as in the studies of other scholars (Shu et al., 2021; Wu et al., 2022). It could, which may be related to the unresolved terrain features by the default surface drag parameterization causing an overestimate of wind speed in particular at low values be argued that the unresolved topographic features produce an additional drag to that generated by vegetation, but their effects are not considered in WRF (Jimenez and Dudhia, 2012) Jimenez and Dudhia, 2012). The model, on the other hand, captures the shift in wind direction. Due to the small change in weak wind, the COR for WS_{10} is not high. To sum up In general, the WRF-Chem model using our configuration has a good capability in simulating $\text{PM}_{2.5}$, O_3 air pollutants and meteorological factors in Chengdu, and thereby the simulations can be used for subsequent analysis.



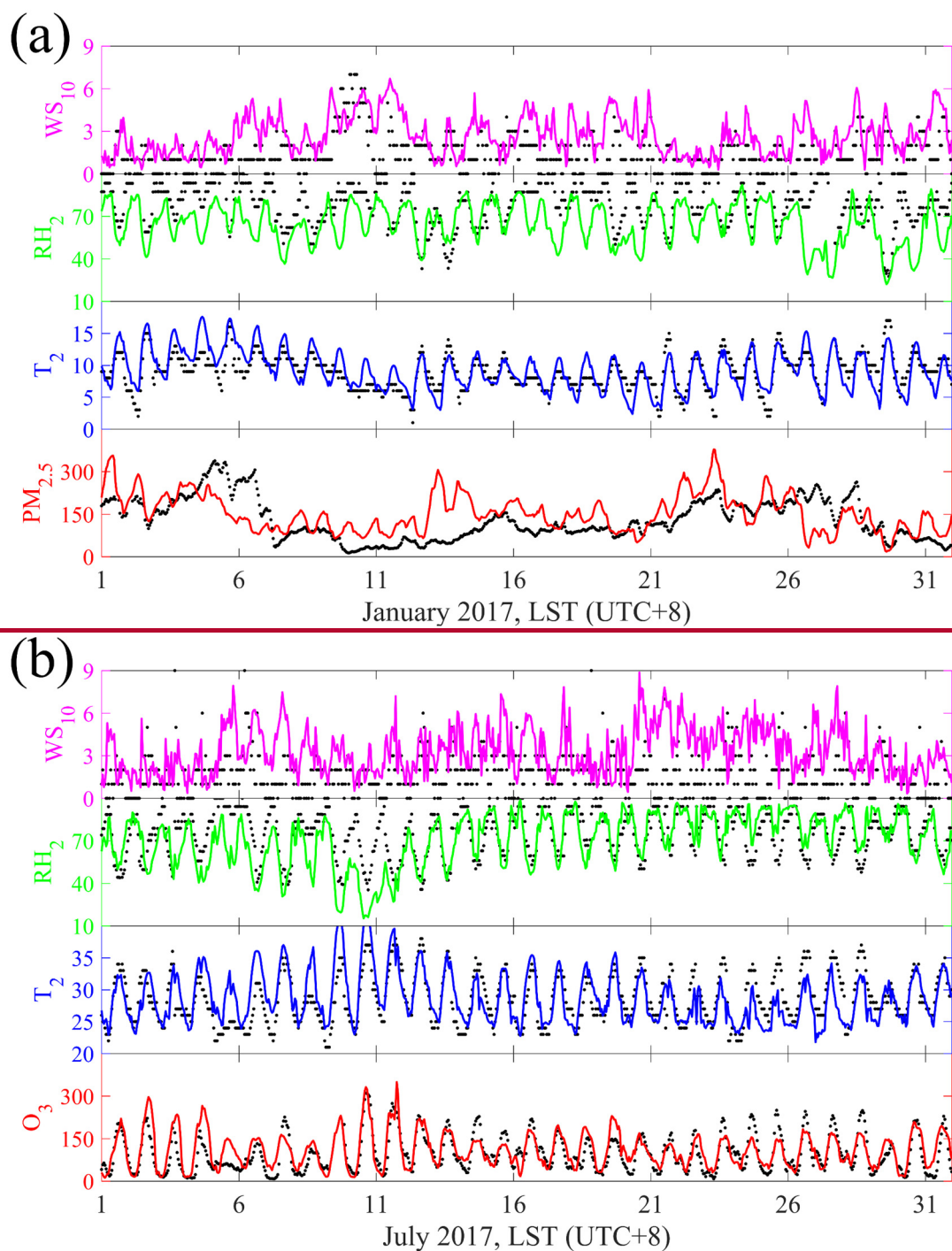
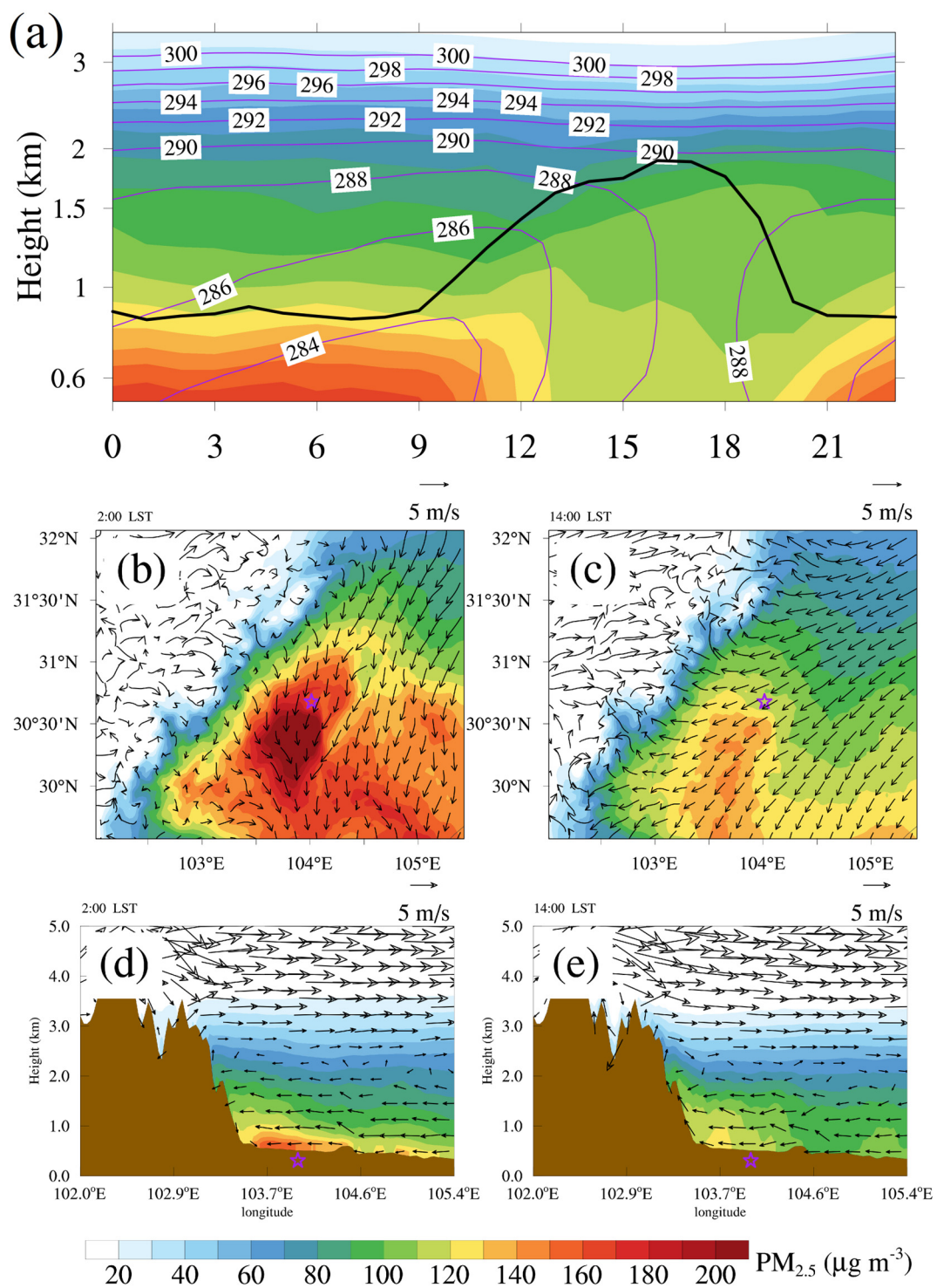


Figure 65. Times series of $PM_{2.5}$, O_3 , T_2 , RH_2 and 10-m wind for (a) January 2017 and (b) July 2017. The black dots are observations and the colored lines are simulations in baseline simulations.

3.3.3 Spatiotemporal variations in $PM_{2.5}$ and O_3

Figure 6 shows the January-averaged spatiotemporal distribution of $PM_{2.5}$ in The spatiotemporal characteristics of $PM_{2.5}$ were first investigated based on the Jan_Base simulation. $PM_{2.5}$ had a diurnal variation with high concentration at night and low concentration at noon, which was contrary to the diurnal variation of the boundary layer height (Figure 7a). The nocturnal atmospheric boundary layer was often characterized by a stable boundary layer. At night, and the boundary layer height was usually only ~320 m low. As a consequence, $PM_{2.5}$ was trapped and maintained on the ground. The daytime atmospheric boundary layer, also known as the convective boundary layer, could develop to ~1300 m. At noon, turbulence in the convective boundary layer could dilute $PM_{2.5}$ concentrations through vertical mixing, resulting in low $PM_{2.5}$ concentrations at surface. Chengdu is on the east side of the Tibetan Plateau, with a large elevation drop exceeding 3000 m over a short horizontal distance (Figure 1a). In this case, the mountain-plain valley breezes wind can easily develop in winter when atmospheric conditions are usually stagnant. During nighttime, the mountain wind was characterized by westerly and downslope flow at lower levels along the eastern slope of the Tibetan Plateau, and are crucial for $PM_{2.5}$ in Chengdu. The $PM_{2.5}$ pollution zone tends to appear in the converging airflows associated with the mountain breezes and can spread hundreds of kilometers (Figure 6a-d). Driven by the near-surface northeasterly winds. Coupled with the prevailing northeasterly wind, $PM_{2.5}$ was uplifted over the eastern windward slope of the Tibetan Plateau, and the $PM_{2.5}$ pollution zone could spread hundreds of kilometers (Figure 7b and d) (Figure 6e-h). The daytime plain wind was nearly a reversal of the nighttime circulation, with easterly and upslope. Then the uphill airflows are restrained and overturned below 3 km, forming a vertical secondary circulation over Chengdu. Governed by the secondary circulation forced by the complex terrain, the southwesterly winds at 3 km can transport $PM_{2.5}$ downward, which could replenish the surface $PM_{2.5}$ and facilitate the accumulation and maintenance of surface $PM_{2.5}$ flow over the Sichuan Basin (Figure 7c and e). The upslope flow could draw $PM_{2.5}$ to a higher elevation, which could also facilitate vertical dispersion of $PM_{2.5}$ during the day. –



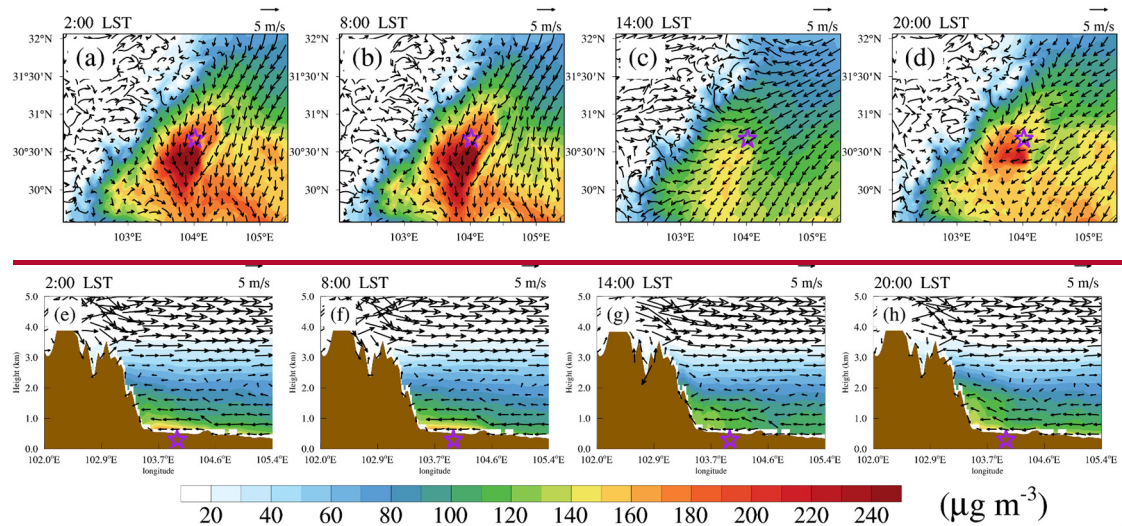
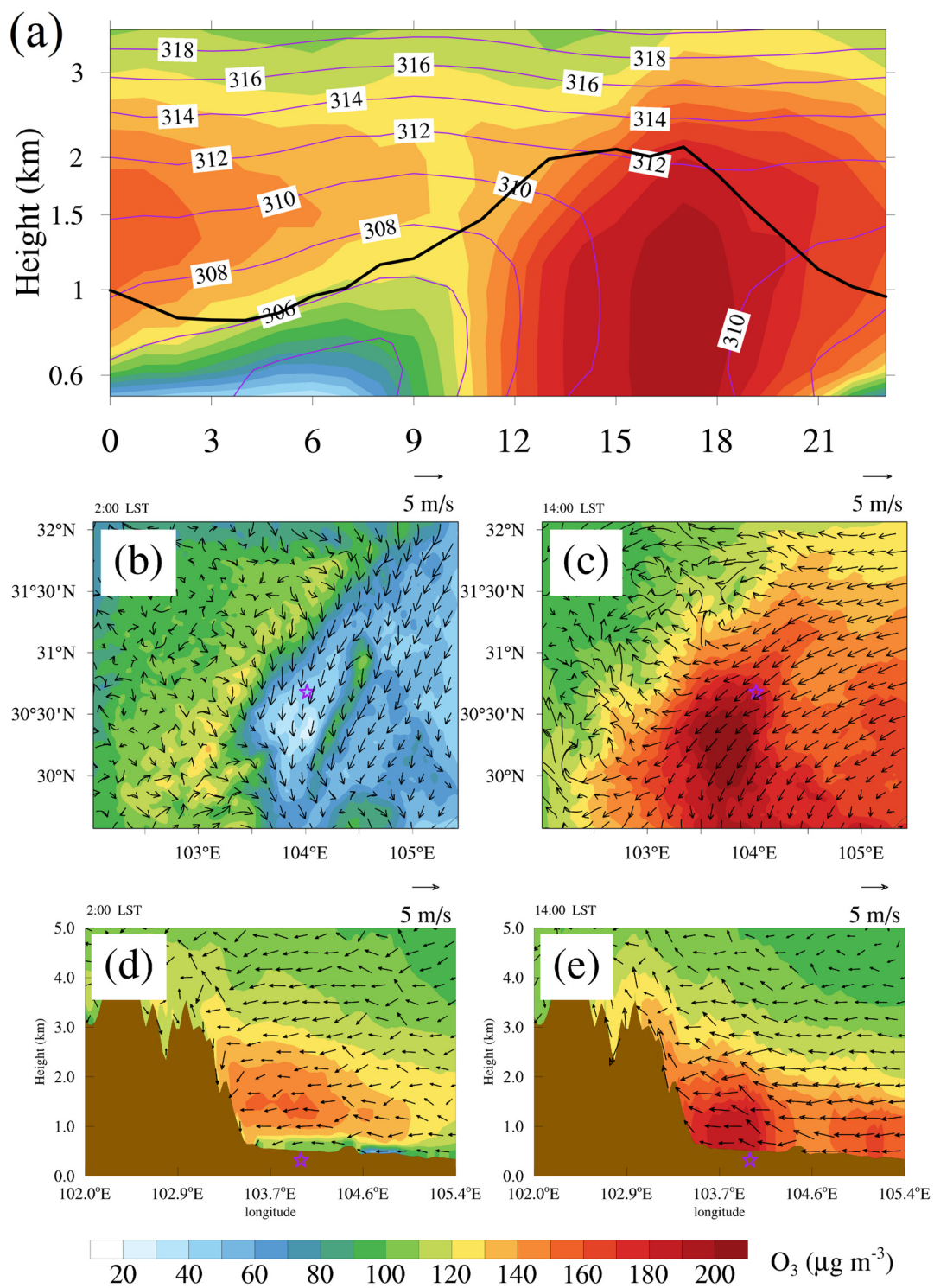


Figure 76. (a-d) Spatial distributions and (e-h) east-west vertical cross sections of $PM_{2.5}$ with wind fields at 2:00, 8:00, 14:00 and 20:00 LST (LST is UTC+8h) in Jan_Base simulation. Purple pentacles show the location of Chengdu. Brown shaded areas represent the terrain. (a) Temporal-vertical cross sections of $PM_{2.5}$, potential temperature and boundary layer height at Chengdu. (b-e) Horizontal spatial distributions of $PM_{2.5}$ with wind vectors at the lowest model level at (b) 2:00 and (c) 14:00 LST. (d-e) east-west vertical cross sections of $PM_{2.5}$ with wind vectors fields at (d) 2:00 and (e) 14:00 LST (LST is UTC+8h). Purple pentacles show the locations of Chengdu. Brown-shaded areas represent the terrain. These results are the monthly average based on from Jan Base simulation.

In terms of O_3 , it exhibits strong diurnal variation with an afternoon maximum and an early morning minimum (Figure 8a-7a-d). After sunrise, the nocturnal residual layer ~~is~~ was destroyed while the convective boundary layer ~~begins to form~~ developed as the surface ~~is~~ heated up on account of the incoming radiation. ~~This leads to downward mixing of O_3 from aloft~~ the high-concentration O_3 in the residual layer was then transported downstream (Hu et al., 2018; Zhan and Xie, 2022). Meanwhile, O_3 ~~could be~~ is also generated by photochemical reactions between volatile organic compounds (VOCs) and NO_x in the presence of sunlight. Through these two pathways, surface O_3 concentration increased rapidly in the morning (Zhan and Xie, 2022) ~~As a consequence, O_3 concentrations increase rapidly from morning to noon~~ (Figure 7b, 7c, 7f and 7g). By noon, O_3 ~~wasean be well~~ was mixed within the convective boundary layer via strong turbulence. Strong

photochemical production and vertical well-mixing could maintain high surface O₃ concentrations until late afternoon. ~~(Figure 7e, 7d, 7g and 7h). The daytime plain wind drove the westward transport of O₃ and aggravated O₃ pollution along the eastern slope of the Tibetan Plateau (Figure 8c and e). After sunset~~ Thereafter, O₃ production ~~ceased~~ decreases ~~as~~ since the intensity of sunlight diminished. ~~After sunset,~~ O₃ concentrations decreased substantially owing ~~due~~ to surface deposition and nitrogen oxide titration ($\text{O}_3 + \text{NO} \rightarrow \text{O}_2 + \text{NO}_2$), and gradually reached their minimum in the early morning (Figure ~~7a, 7d, 7e and 7h~~ 8b). But O₃ in the nocturnal residual layer was still at a high level with values of more than 1640 $\mu\text{g m}^{-3}$. The nighttime mountain wind could carry air containing rich O₃ eastward downslope and enhanced O₃ concentrations aloft over the eastern slope of the Tibetan Plateau (Figure 8d). Compared with the Jan_Base simulation, the secondary circulation forced by the complex terrain is not obvious. In addition Compared with the Jan_Base simulation, O₃ with a concentration of about $100 \mu\text{g m}^{-3}$ had always existed over the Tibetan Plateau where, ~~but~~ PM_{2.5} concentrations were ~~there are~~ quite low, indicating. ~~This indicates~~ that the background concentration of O₃ was ~~is~~ much higher than that of PM_{2.5}. ~~This~~ which ~~can~~ may pose a huge challenge to O₃ pollution control.



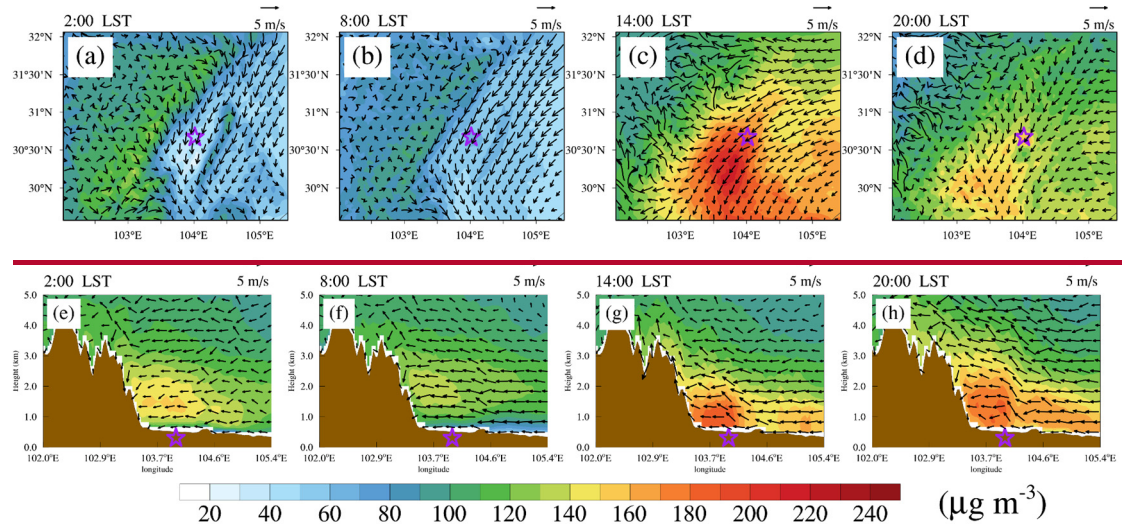
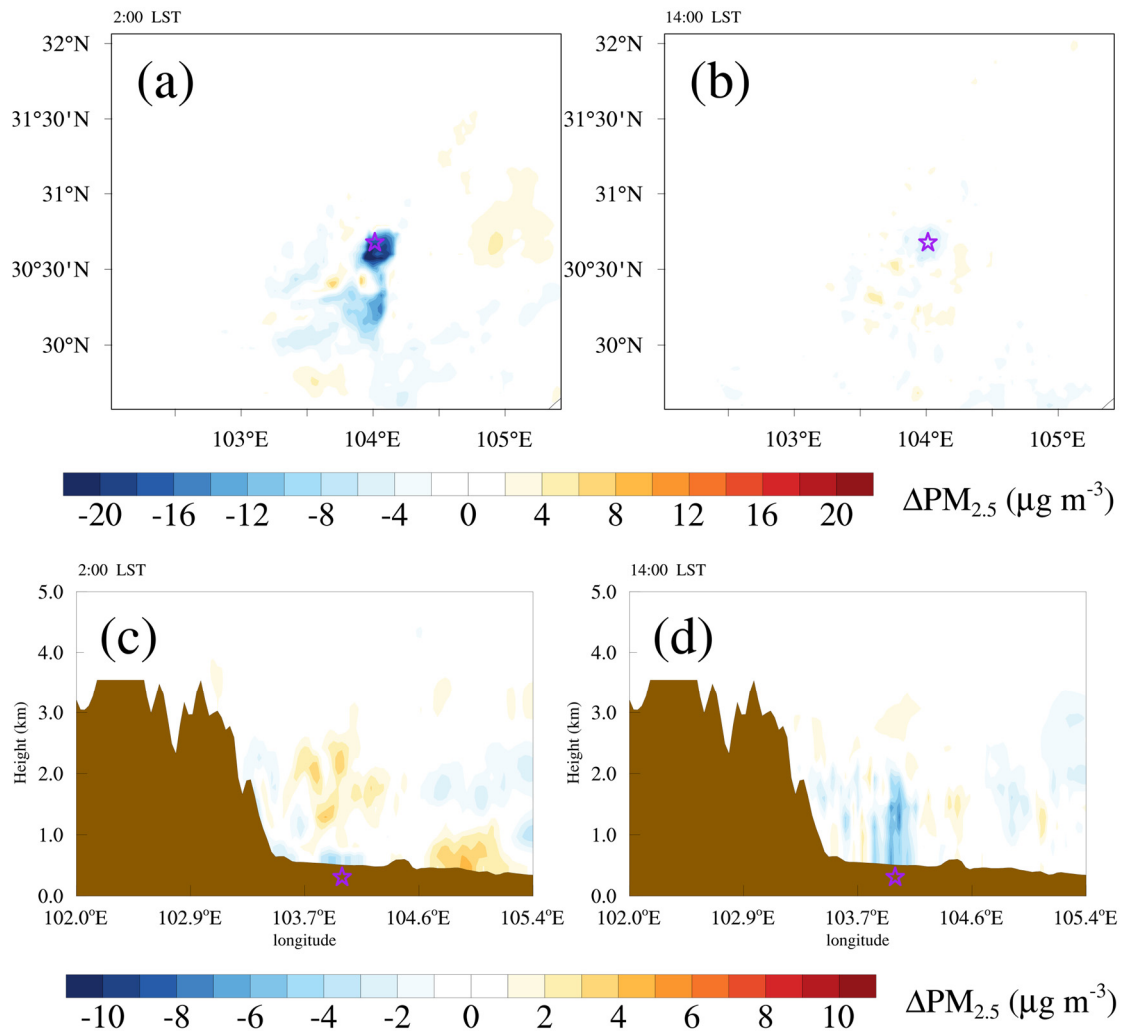


Figure 87. (a) Temporal-vertical cross sections of O_3 , potential temperature and boundary layer height at Chengdu. (b-e) Spatial-Horizontal distributions and (d-e) east-west vertical cross sections of O_3 with wind vectors fields at the lowest model level at (b) 2:00 and (c) 14:00 LST (LST is UTC+8h). East-west vertical cross sections of O_3 with wind vectors at (d) 2:00 and (e) 14:00 LST. Purple pentacles show the locations of Chengdu. Brown-shaded areas represent the terrain. These results are the monthly average based on July Base simulation. These results are from July Base simulation. (a-d) Spatial distributions and (e-h) east-west vertical cross sections of O_3 with wind fields at 2:00, 8:00, 14:00 and 20:00 LST (LST is UTC+8h) in July Base simulation. Purple pentacles show the location of Chengdu. Brown-shaded areas represent the terrain.

3.3.4 Impacts of urban land use expansion on $PM_{2.5}$ and O_3

Modification of urban land use changes surface dynamic and thermal characteristics, ~~and thereby affects the transportation and dispersion of air pollutants affecting the exchange of energy, moisture and momentum and hence altering urban meteorology and air quality.~~ Figure 8 shows the differences in $PM_{2.5}$ between Jan_Base and Jan_noCD simulations (Jan_Base minus Jan_noCD). As illustrated in Figure 9, Results show that ~~surface~~ $PM_{2.5}$ concentrations in Jan_Base simulation ~~were~~ are lower than those ~~in~~ lower at all times compared with Jan_noCD simulation, ~~with the monthly average concentrations decreased by 10.81-7 $\mu g m^{-3}$ (7.6%) (Figure 8a-d).~~ Moreover, ~~the decrease in $PM_{2.5}$ concentrations was~~ larger during the nighttime than

during the daytime. Specially, The monthly averages surface PM_{2.5} concentrations could decrease by 135.90 $\mu\text{g m}^{-3}$ (8.6%) at 2:00 LST (LST is UTC+8h) and only -3.02 $\mu\text{g m}^{-3}$ (2.6%) at 14:00 LST (Figure 9a and b). The decrease in surface PM_{2.5} concentrations was mainly attributed to the modification of the boundary layer height. Urban land use can enhance surface heating and then increases leading to an increase in air temperature, known as the urban heat island. The vertical air movement is then enhanced by the warming up of surface air temperature, resulting in an increase in the boundary layer height (Figure S1), which facilitates the vertical diffusion of surface PM_{2.5}. PM_{2.5} concentrations increased by 2~6 $\mu\text{g m}^{-3}$ in the upper boundary layer (~1 km above the surface) (Figure 9c and d), further confirming this point.



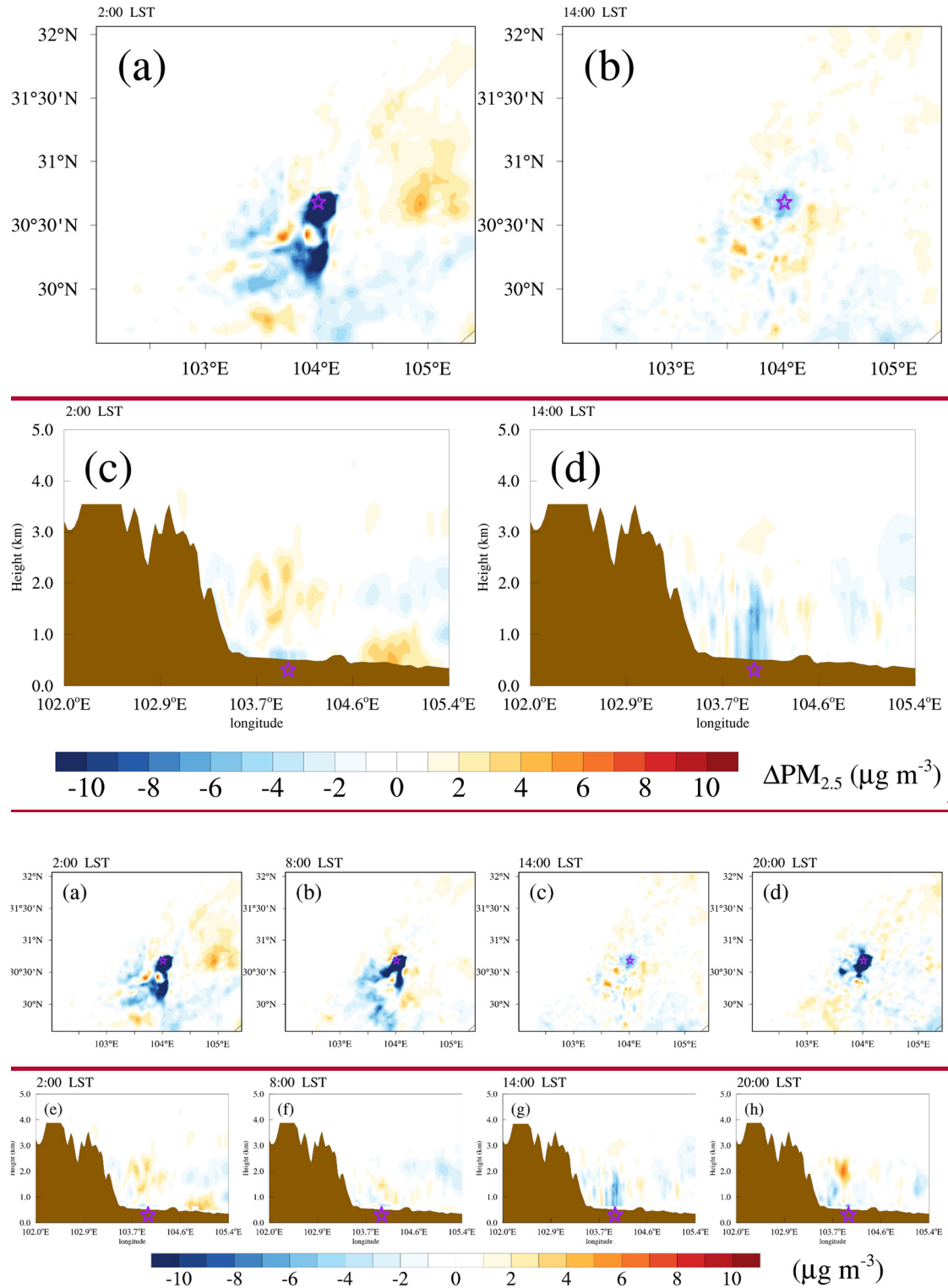
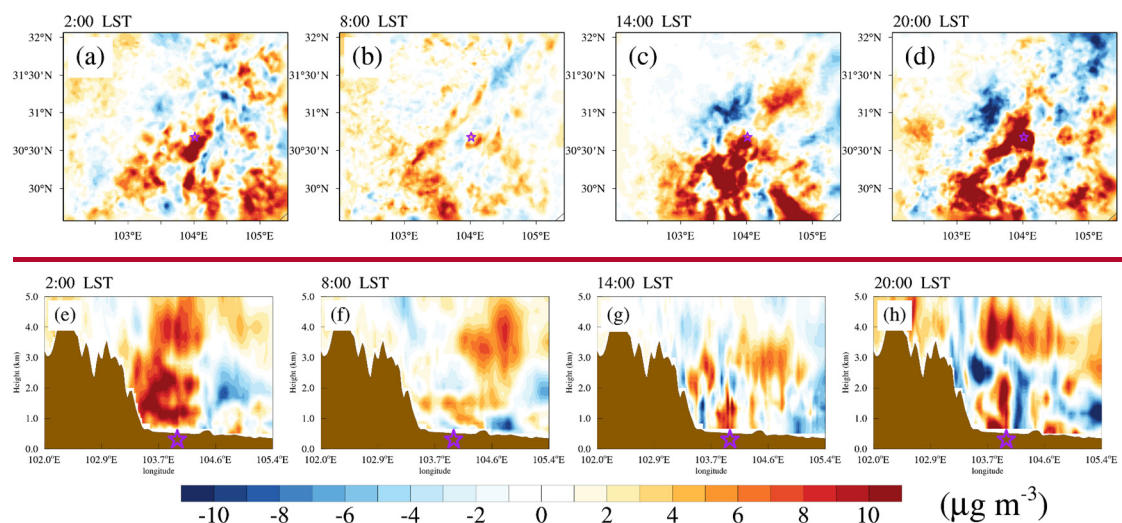
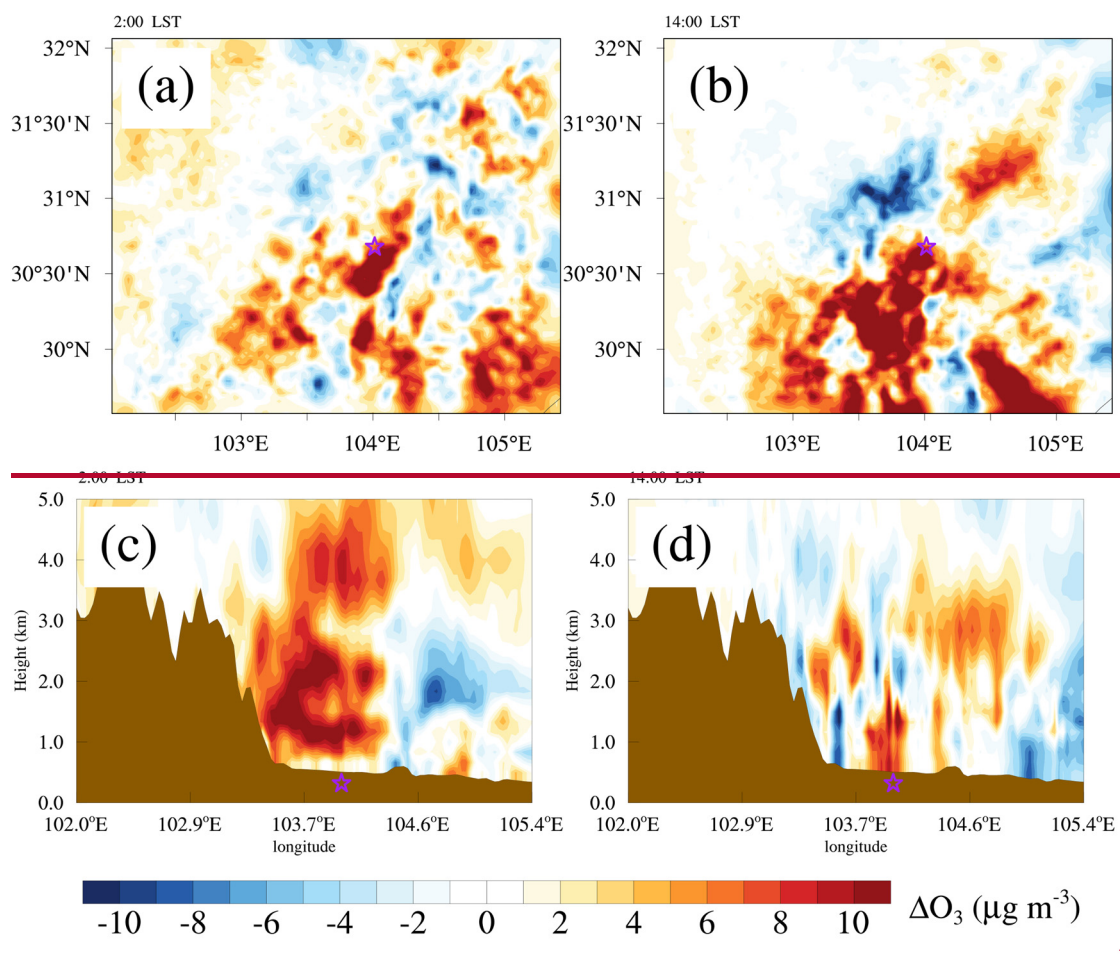


Figure 98. (a-d) Horizontal spatial distributions and (e-h) east-west vertical cross sections of the differences in $\text{PM}_{2.5}$ at the lowest model level at (a) 2:00 and (b) 14:00 LST between Jan_Base and Jan_noCD simulations (Jan_Base minus Jan_noCD). East-west vertical cross sections of the difference in $\text{PM}_{2.5}$ at (c) 2:00 and (d) 14:00 LST. Purple pentacles show the

location of Chengdu. Brown-shaded areas represent the terrain. These results are the difference between the monthly average of Jan Base and Jan noCD simulations (Jan Base minus Jan noCD).

O₃ is a secondary air pollutant that is not only related to meteorological conditions but also to its precursors (VOCs and NO_x). Due to the increase in upward air movement and boundary layer height induced by urban land use (Figure S2), like PM_{2.5}, ~~PM_{2.5} and~~ NO_x concentrations also decreased near the surface ~~but increase in the upper boundary layer~~ (Liao et al., 2015; Zhu et al., 2017). The decrease in NO_x near the surface resulted in ~~results in~~ an increase in surface O₃ at night since the NO_x titration wasis ~~wasis~~ weakened (Figure 109a and ~~dc~~). Although the elevated boundary layer diluteds O₃ concentrations to some extent, the nighttime O₃ concentrations wereare mainly dominated by chemical effects and eventually increased ~~by 15a maximum of 25.68~~ $\mu\text{g m}^{-3}$ (16.0%) at 2:00 LST (Figure 10a). During ~~the~~ daytime, the increased air temperature wasis ~~wasis~~ conducive to the photochemical production of O₃, and the well-developed convective boundary layer favores ~~the~~ the vertical mixing of O₃. O₃ concentrations would ~~ill~~ also increase (Figure 109b and ~~de~~), with the ~~the~~ monthly average value of 54.4 $\mu\text{g m}^{-3}$ (4.5%) at 14:00 LST. in Chengdu. ~~Since high O₃ concentrations were mainly concentrated in the afternoon~~ Finally, the monthly average MDA8 O₃ concentrations ~~in July can~~ finally increased by 10.6 $\mu\text{g m}^{-3}$ (6.0%) due to the effects of urban expansion.





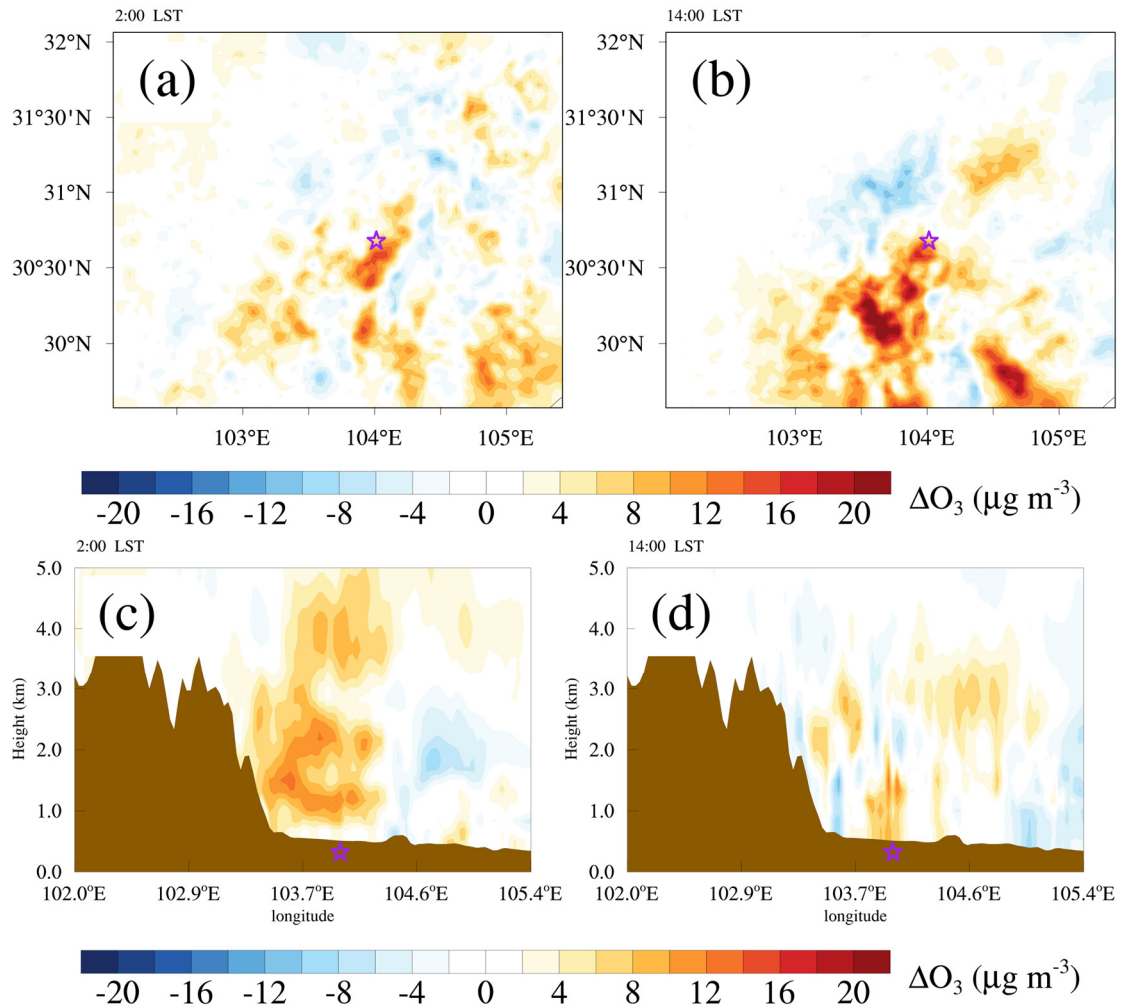
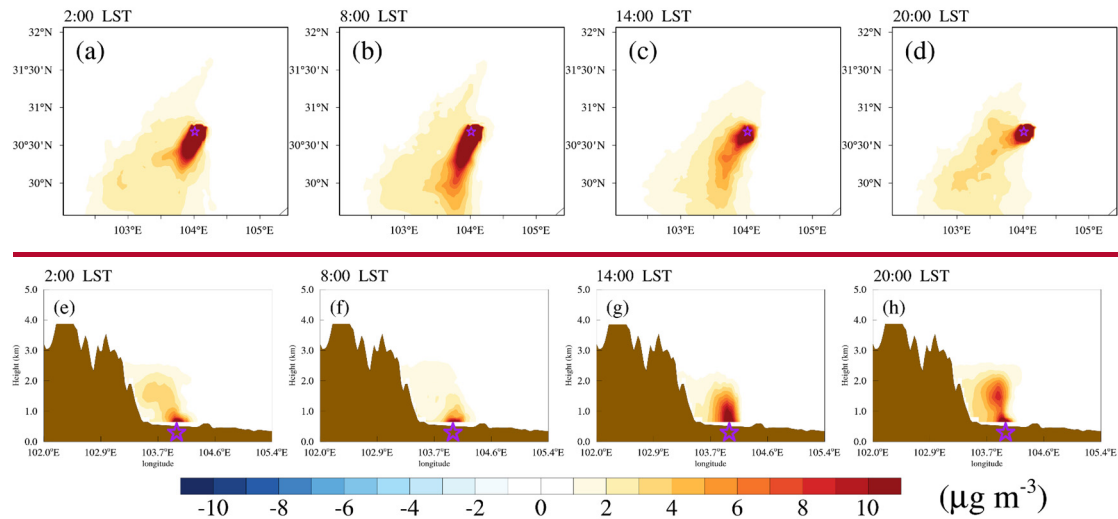


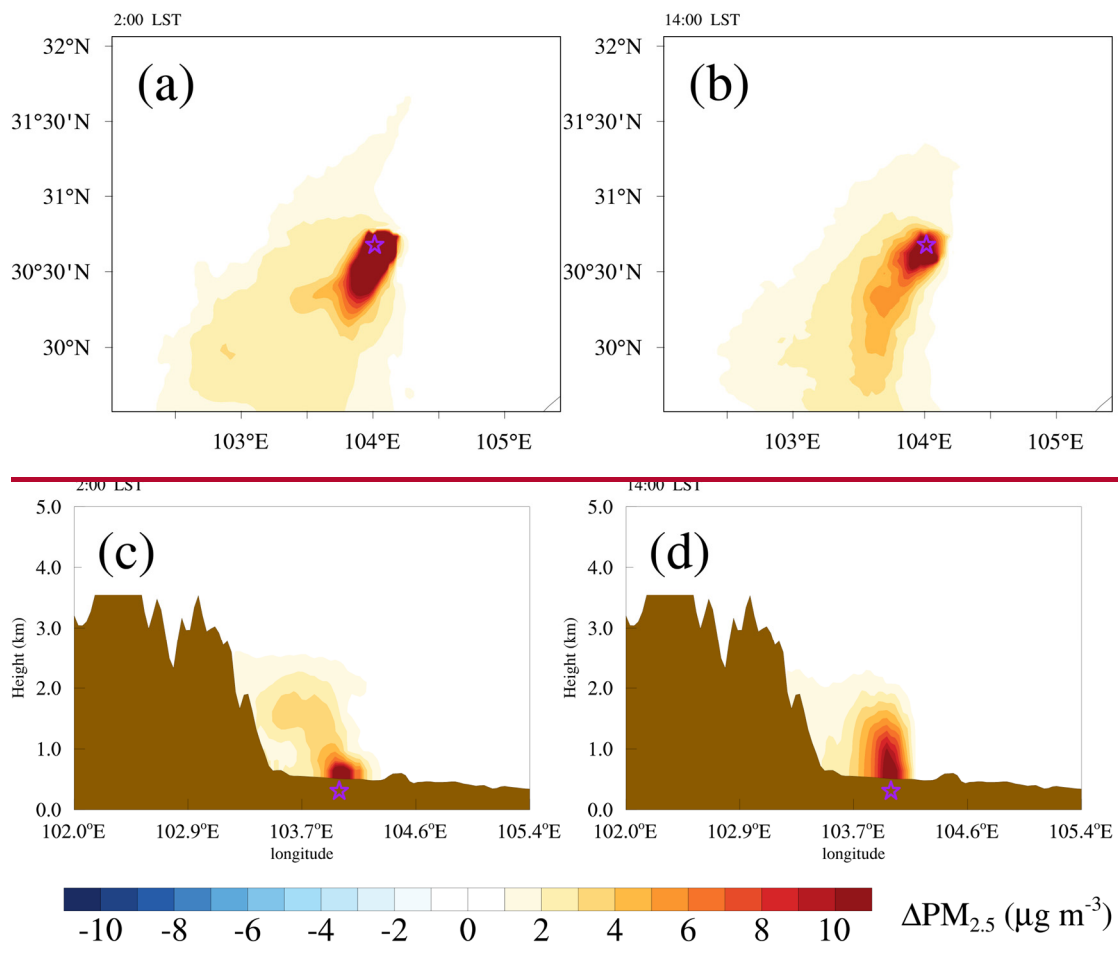
Figure 10. Horizontal distributions of the differences in O_3 at the lowest model level at (a) 2:00 and (b) 14:00 LST. East-west vertical cross sections of the difference in O_3 at (c) 2:00 and (d) 14:00 LST. Purple pentacles show the location of Chengdu. Brown-shaded areas represent the terrain. These results are the difference between the monthly average of July Base and July noCD simulations (July Base minus July noCD).

3.3.5 Impacts of anthropogenic emissions on $PM_{2.5}$ and O_3

Air pollutants become part of the air once released, and they do not have a direct effect on airflows like temperature or radiation. Rising anthropogenic emissions of air pollutants and their precursors can significantly increase ambient air pollution. Therefore, the impacts of anthropogenic

emissions are more intuitive than urban land use expansion. Figure 11 shows the differences in PM_{2.5} between the monthly average of Jan_Base and Jan_noEmi simulations (Jan_Base minus Jan_noEmi). PM_{2.5} concentrations in Jan_Base simulation were significantly higher than those in Jan_noEmi simulations, with the monthly average concentration increasing by 236.96 $\mu\text{g m}^{-3}$ (16.8%), more than twice the difference between Jan_Base and Jan_noCD simulations. Furthermore, the increases in PM_{2.5} concentrations appeared throughout the boundary layer (Figure 11c and d-h) and could extend downstream for hundreds of kilometers (Figure 11a and b-d), indicating that reducing anthropogenic emissions is an effective way to reduce PM_{2.5} concentrations.





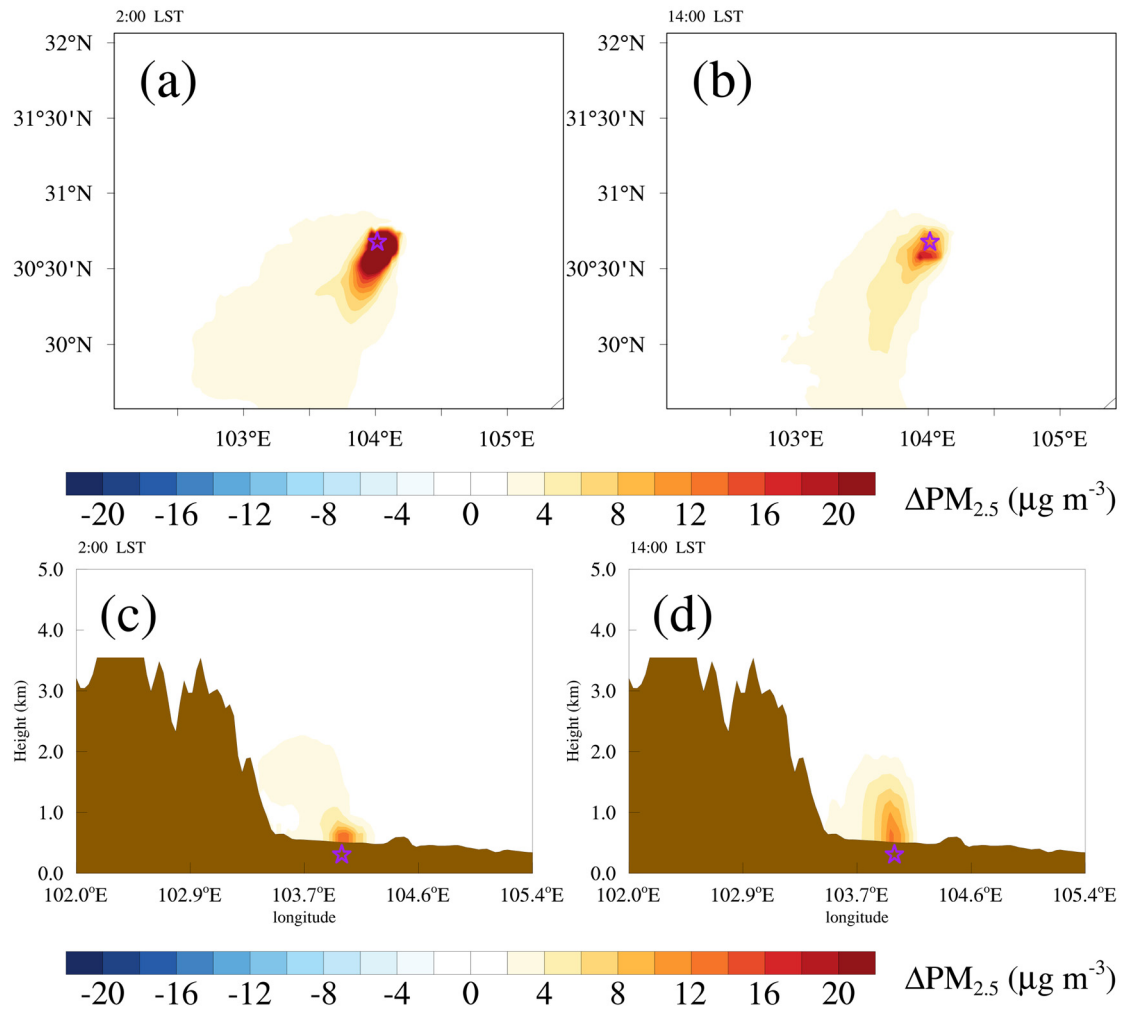
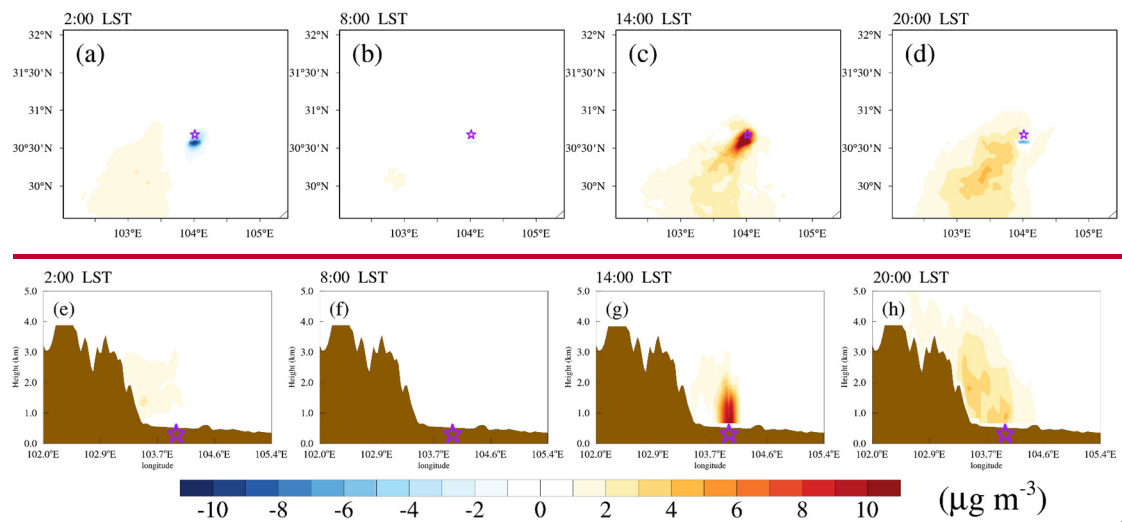
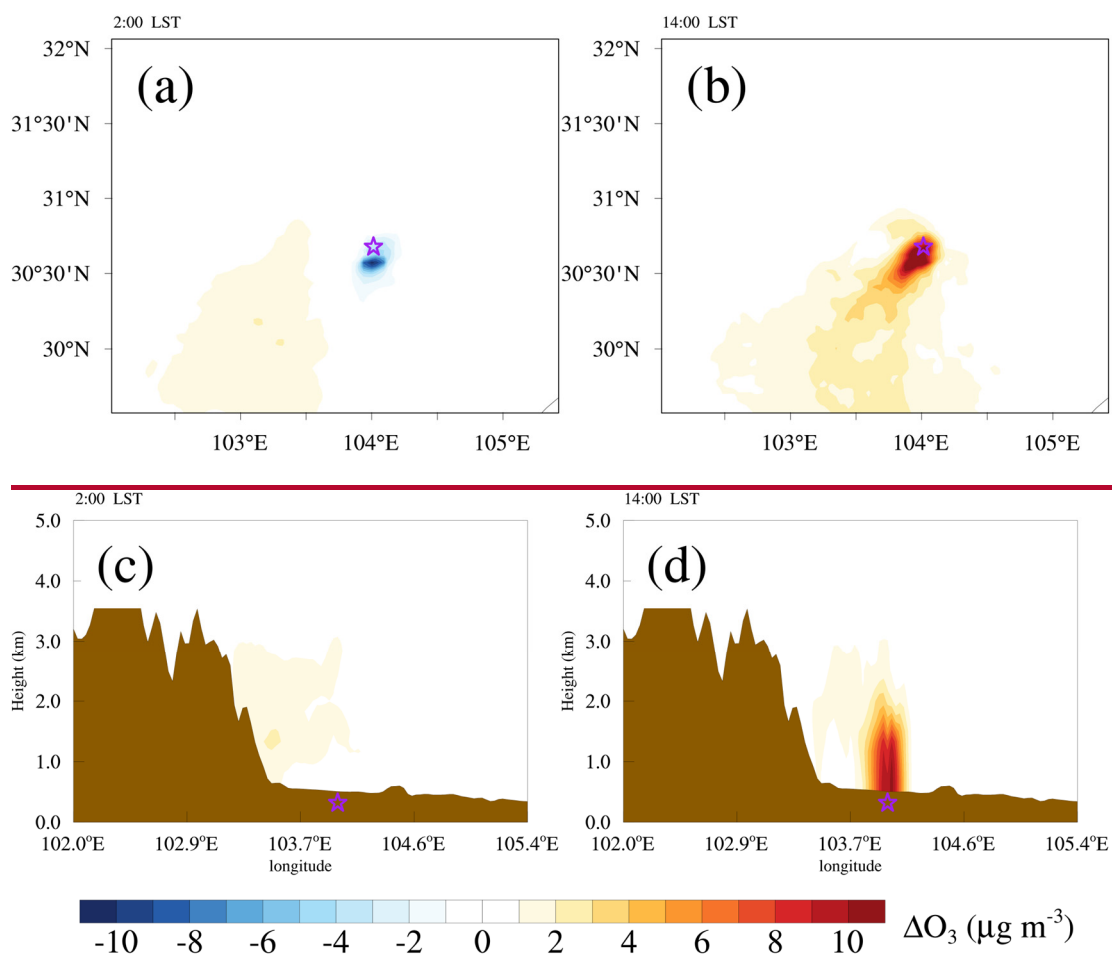


Figure 10. Same as Figure 9, but for the difference between the monthly average of Jan_Base and Jan_noEmi simulations (Jan_Base minus Jan_noEmi). (a-d) Spatial distributions and (e-h) east-west vertical cross sections of the differences in $PM_{2.5}$ between Jan_Base and Jan_noEmi simulations (Jan_Base minus Jan_noEmi). Purple pentacles show the location of Chengdu. Brown shaded areas represent the terrain.

As for O_3 , O_3 concentrations in July_Base simulation ~~were~~ only $15.68 \mu g m^{-3}$ (1.4%) higher than those in July_noEmis simulation at 14:00 LST ~~due to the abundance of O_3 precursors~~ (Figure 11e12b and d), which was much smaller than the change in $PM_{2.5}$. However, O_3 concentrations decrease by $3.4 \mu g m^{-3}$ at 2:00 LST (Figure 11a). This phenomenon may be related to the non-linear sensitivity of O_3 to VOCs and NO_x precursor emissions. O_3 formation regimes can be often classified into VOC-limited, NO_x -limited and transition regimes depending on the ratio of VOCs and NO_x (Jin et al., 2020; Lu et al., 2019). At low VOC/ NO_x ratios (VOC-limited regime, usually

in urban areas), reducing the concentrations of NO_x would even lead to an increase in O₃ formation. Considering Chengdu remained VOC-limited regime during 2013 to 2020 (Tian et al., 2018; Wang et al., 2022), the effects of reducing NO_x emissions may be partially offset by changes in VOCs, and thereby a reasonable regulation framework that involves joint control of NO_x and VOC emissions is necessary to alleviate O₃ pollution. On the other hand, the presence of anthropogenic emissions reduced O₃ concentrations by 3.0 µg m⁻³ (3.1%) at 2:00 LST. Finally, the monthly average ~~Apart from the amount of anthropogenic emissions, a reasonable emission reduction path is also necessary to alleviate O₃ pollution.~~ Since O₃ concentrations increase during the daytime, MDA8 O₃ concentrations in July_Base simulation ~~were~~ are still 4.8 µg m⁻³ (2.7%) higher than those in July_noEmis simulation.





611

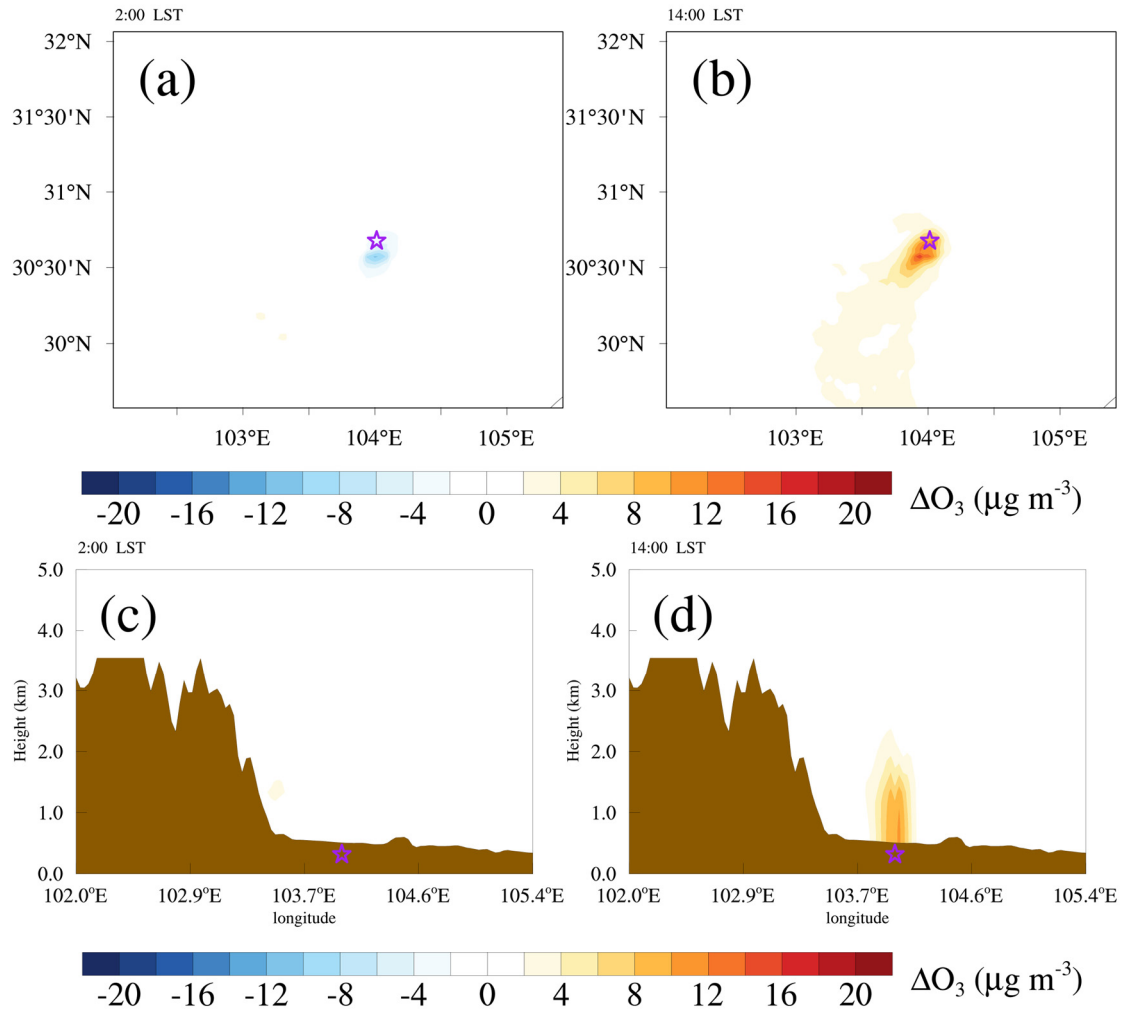


Figure 12. Same as Figure 10, but for the difference between the monthly average of July Base and July noEmi simulations (July Base minus July noEmi). (a-d) Spatial distributions and (e-h) east-west vertical cross sections of the differences in O₃ between July Base and July noEmi simulations (July Base minus July noEmi). Purple pentacles show the location of Chengdu. Brown shaded areas represent the terrain.

3.4 Health risks caused by urbanization

According to the above results, urban ~~land use expansion could~~ decrease the monthly average of surface PM_{2.5} concentrations by 104.87 $\mu\text{g m}^{-3}$ (7.6%) but increase the monthly average of MDA8 O₃ concentrations by 10.6 $\mu\text{g m}^{-3}$ (6.0%). On the other hand, anthropogenic emissions ~~could~~ increase surface both PM_{2.5} by 26.6 $\mu\text{g m}^{-3}$ and MDA8 O₃ concentrations, with the monthly average values of 23.9 $\mu\text{g m}^{-3}$ (16.8%) and by 4.8 $\mu\text{g m}^{-3}$ (2.7%), respectively. We then calculate the changes in premature mortalities under different simulation scenarios to assess the health risks from

~~changes in PM_{2.5} and O₃ concentrations to access the health risks from changes in PM_{2.5} and O₃~~
~~concentrations~~. As shown in Figure 132, the premature mortalities from ANAC, CVD, RD and
COPD due to PM_{2.5} decreased ~~d~~ by 1871 (95%CI: 129~200, or about 6.9%), 45 (95%CI: 34~53, or
~~about 6.7%), 22 (95%CI: 16~27, or about 6.5%)~~2 (6.9%), 47 (6.5%), 23 (6.4%) and 24 (6.1%) and
~~23 (95%CI: 17~26, or about 6.2%)~~ in January 2017 with the existence of Chengdu. While
anthropogenic emissions in Chengdu increased ~~d~~ premature mortalities from ANAC, CVD, RD and
COPD due to PM_{2.5} by 424 (16.0%), 111 (15.4%), 55 (15.2%) and 56 (14.3%) 388 (95%CI: 291~456,
~~or about 15.7%), 102 (95%CI: 77~121, or about 15.1%), 51 (95%CI: 35~62, or about 15.0%) and~~
~~52 (95%CI: 39~60, or about 14.1%), respectively~~. With regard to O₃, premature mortalities from ~~the~~
O₃-induced diseases all increased ~~d~~ when urban land use and anthropogenic emissions ~~were~~are taken
into account. Urban ~~land use expansion~~ leads to an increase ~~in~~of premature mortalities from ANAC,
CVD, RD and COPD due to O₃ by 203 (95%CI: 122~268, or about 9.5%9.5%), 51 (95.4%CI: 22~71,
~~or about 9.4%), 18 (95%CI: -14~35, or about 10.0%0.0%) and 17 (95.7%CI: -15~33, or about~~
~~9.7%)~~ in July 2017, ~~respectively~~. When anthropogenic emissions in Chengdu ~~were~~are turned on,
premature mortalities from ANAC, CVD, RD and COPD due to O₃ ~~can~~ increased ~~d~~ by 87 (95%CI:
~~54~112, or about 4.1%4.1%), 22 (95%CI: 10~29, or about 4.1%4.1%), 8 (95.4%CI: -7~14, or~~
~~about 4.4%) and 7 (95.4%CI: -7~13, or about 4.0%), respectively~~. In summary, ~~affected by urban~~
~~expansion and anthropogenic emissions, changes in the~~ total premature mortalities due to PM_{2.5}
~~and O₃ changed by~~are about ~~—6.9% and 9.5~~16.0% ~~affected by urban expansion, and these values~~
~~changed to, due to O₃ are about 15.7~~9.5% and ~~4.1~~4.1% ~~affected by emissions growth~~. The effects
of urban expansion on health risks are in the same order (1/2 to 2 times) as those induced by
anthropogenic emissions.

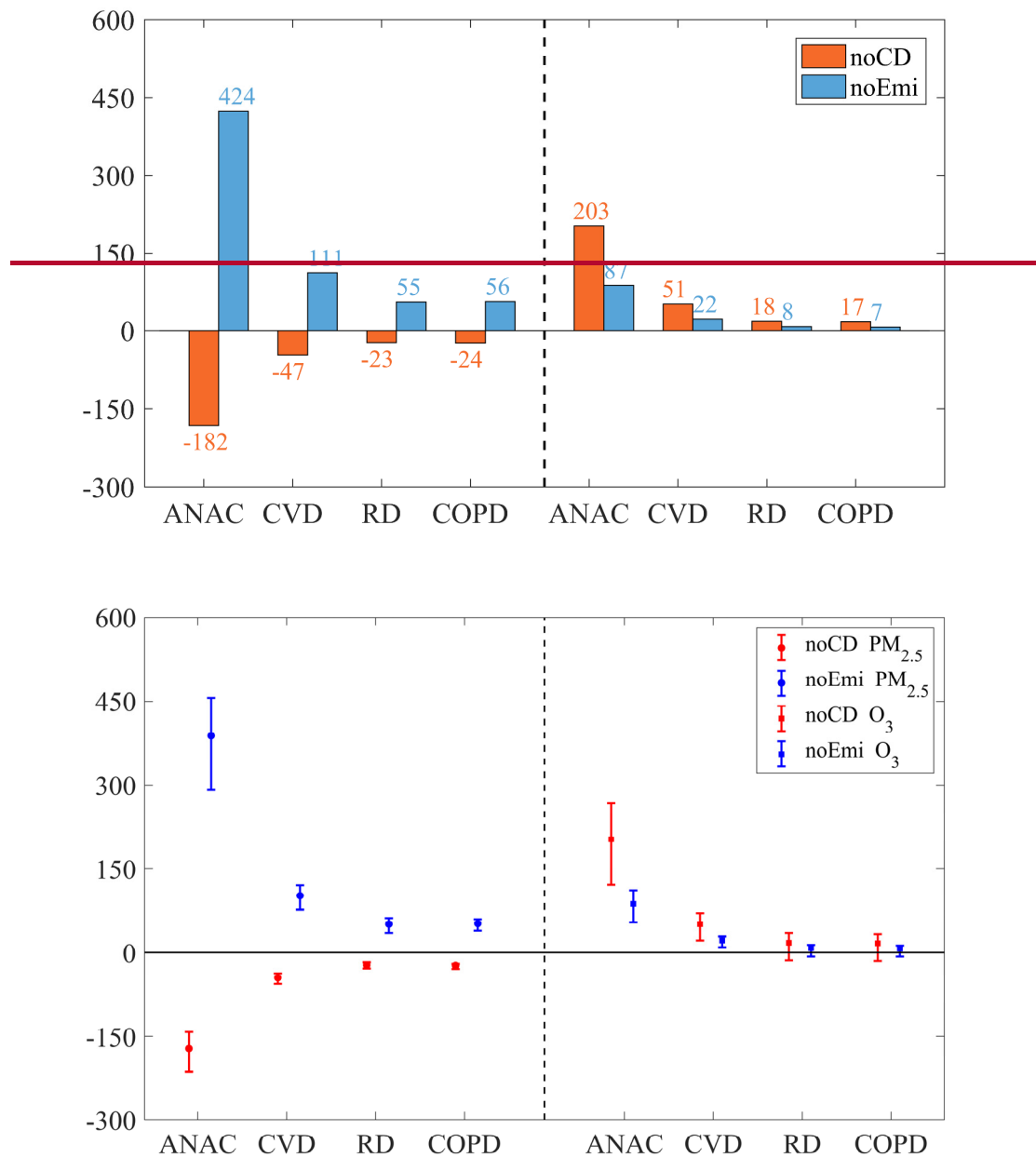


Figure 132. Differences in premature mortality from ANAC, CVD, RD and COPD due attributed to PM_{2.5} (left of dotted line) and O₃ (right of dotted line) exposure between baseline and sensitivity simulations. The red bars are the differences between Jan_Base and Jan_noCD simulations (Jan_Base minus Jan_noCD), and the differences between July_Base and July_noCD simulations (July_Base minus July_noCD). The blue bars are the differences between Jan_Base and Jan_noEmi simulations (Jan_Base minus Jan_noEmi), and the differences between July_Base and July_noEmi simulations (July_Base minus July_noEmi).

4 Conclusions

With the development in urbanization, urban land use and anthropogenic emissions increase, which affects urban air quality and then health risks of air pollutants. In this study, the impacts of urban ~~land use and anthropogenic emissions~~ization on air quality and the ~~related~~corresponding health risks in Chengdu, a highly urbanized city with severe air pollution and complex terrain, are quantified. Management of urban air pollution is usually achieved by reducing anthropogenic emissions. ~~Thus, So—~~ the ~~effects~~impacts of urban expansion ~~have been~~are also ~~further~~ compared with ~~those of emissions growth~~anthropogenic emissions on health risks.

Chengdu is suffering from severe PM_{2.5} and O₃ pollution in recent years. There ~~were~~are 97, 101, 68, 53, 33, 43 and 37 PM_{2.5} pollution episodes, and 61, 48, 42, 40, ~~4226~~, ~~7150~~ and ~~4827~~ O₃ pollution episodes ~~in Chengdu~~ from 2015 to 2021. Severe PM_{2.5} and O₃ pollution posed huge health risks. The 7-year annual ~~average of~~ premature mortalities from ANAC, CVD, RD and COPD due to PM_{2.5} ~~were~~are 9386 (95%CI: 6542~11726), 2609 (95%CI: 1788~3384), 1321 (95%CI: 804~1840) and 1485 (95%CI: 941~1983), ~~those~~ due to O₃ ~~were~~are ~~8506 (95%CI: 4817~11882)~~7743, ~~2175 (95%CI: 863~3320)~~1981, ~~713 (95%CI: -492~1664)~~648 and ~~693 (95%CI: -517~1617)~~30. PM_{2.5} and O₃ pollution had~~ve~~ different seasonal preferences. ~~Owing~~Due to the ~~secondary circulation driven by complex terrain blocking of air~~ and the frequent temperature inversion, PM_{2.5} pollution tended~~s~~ to appear in cold months (November to February). ~~While~~ O₃ pollution ~~was~~is likely to occur in warm months (April to August) because of high temperature and strong sunlight dominated by high-pressure systems. PM_{2.5} ~~has a diurnal variation with high~~ concentrations ~~were high~~ at night ~~and but~~ low ~~concentrations~~ at noon, ~~which was affected by~~contrary to the boundary layer height. ~~While~~ O₃ exhibited~~s~~ strong diurnal variation with an afternoon maximum and an early morning minimum, which ~~was~~is related to photochemical reactions during ~~the~~ daytime and nitrogen oxide titration at night.—

The urban land use of Chengdu ~~was~~is replaced by cropland in the WRF-Chem model to examine the impacts of urban expansion. Urban ~~land use~~expansion leads to an increase in air temperature and boundary layer height, and decreased~~s~~ surface PM_{2.5} concentrations by ~~10.81.7~~ $\mu\text{g m}^{-3}$ (7.6%) in January 2017. ~~Higher temperature and boundary layer height increased O₃~~As for O₃, ~~the surface concentration increases by 4.4 $\mu\text{g m}^{-3}$ at noon due~~ concentrations via ~~to~~ stronger photochemical reactions and better vertical mixing ~~during daytime. During nighttime, dominated~~

by the weakened chemical NO_x titration, O₃ concentrations ~~also~~ increased by 25.8 μg m⁻³ at midnight since the NO_x titration is weakened. MDA8 O₃ concentrations could finally increase by 10.6 μg m⁻³ in July 2017 (6.0%). In this case, when urban land use was taken into account. In this case, the premature mortalities from ANAC, CVD, RD and COPD attributed due to PM_{2.5} exposure decreased by 171 (95%CI: 129~200, or about 6.9%), 182 (6.9%), 47 (6.5%), 23 (6.4%) and 24 (6.1%), but those due attributed to O₃ exposure increased by 203 (95%CI: 122~268, or about 9.5%), 203 (9.1%), 51 (9.4%), 18 (10.0%) and 17 (9.7%). Anthropogenic emissions increased surface PM_{2.5} significantly with the monthly average concentration increasing by 236.96 μg m⁻³ (16.8%), more than twice the difference caused by urban land use expansion. Owing Due to the non-linear sensitivity of O₃ to its precursors, O₃ concentrations increased during the daytime at noon but decreased at night. In particular, the monthly average O₃ concentrations increased by 15.68 μg m⁻³ (1.4%) at 14:00 LST but decreased by 3.04 μg m⁻³ (3.1%) at 2:00 LST with anthropogenic emissions in Chengdu. Since O₃ concentrations in daytime were much higher than those at night, the MDA8 O₃ concentrations still increased by 4.8 μg m⁻³ (2.7%). As a consequence, the premature mortalities from ANAC due, CVD, RD and COPD attributed to PM_{2.5} exposure increased by 388 (95%CI: 291~456, or about 15.7%), 424 (16.0%), 111 (15.4%), 55 (15.2%) and 56 (14.3%), and those due attributed to O₃ exposure increased by 87 (95%CI: 54~112, or about 4.1%) with anthropogenic emissions in Chengdu 87 (4.1%), 22 (4.1%), 8 (4.4%) and 7 (4.0%).

Our results show that the impacts of urban expansion (about -6.9% for PM_{2.5} and about 9.5% for O₃) are in the same order (1/2 to 2 times) as those induced by emissions growth (about 15.7% for PM_{2.5} and about 4.1% for O₃) on air pollutants. This suggests that although the focus of air quality management is traditionally to regulate emissions, urban planning is an ancillary option and should also be considered in future air pollution strategies.

Data Availability Statement.

Air quality monitoring data are acquired from the official NEMC real-time publishing platform (<http://106.37.208.233:20035/>). Meteorological data are taken from the website of the University of Wyoming (<http://weather.uwyo.edu/>). The NCEP global final analysis-FNL data were taken from the NCEP (<https://doi.org/10.5065/D6M043C6/>). The MEIC data are accessible at <http://meicmodel.org/>. These data can be downloaded for free as long as you agree to the official

instructions.

Author contributions.

CZ and MX had the original ideas, designed the research, collected the data and prepared the original draft. CZ did the numerical simulations and carried out the data analysis. MX acquired financial support for the project leading to this publication. HL, BL and ZW collected the data. TW, BZ, ML and SL reviewed the initial draft and checked the language of the original draft.

Competing interests.

The contact author has declared that neither they nor their co-authors have any competing interests.

Acknowledgements.

We are grateful to NEMC for the air quality monitoring data, to NCDC for the meteorological data, to NCEP for global final analysis fields and to Tsinghua University for the MEIC inventories. The numerical calculations were performed on the Blade cluster system in the High-Performance Computing and Massive Data Center (HPC&MDC) of School of Atmospheric Sciences, Nanjing University. We thank the anonymous reviewers for their constructive comments and suggestions.

Financial support.

This work was supported by the National Nature Science Foundation of China (grant no. 42275102), the open research fund of Chongqing Meteorological Bureau (KFJJ-201607) and the Natural Science Foundation of Jiangsu Province (grant no. BK20211158).~~This work was supported by the open research fund of Chongqing Meteorological Bureau (KFJJ-201607), the Natural Science Foundation of Chongqing (este2021jcyj-msxmX1007), the Chongqing Science and Technology Commission technology innovation and application demonstration project (este2018jszx-zdyfxmX0003) and Innovation Team Fund of Southwest Regional Meteorological Center, China Meteorological Administration.~~

References

749 Aneja, V. P., Mathur, R., Arya, S. P., Li, Y. X., Murray, G. C., and Manuszak, T. L.: Coupling the
750 vertical distribution of ozone in the atmospheric boundary layer, *Environ. Sci. Technol.*, 34,
751 2324-2329, <https://doi.org/10.1021/es990997+>, 2000.

752 Anenberg, S. C., Horowitz, L. W., Tong, D. Q., and West, J. J.: An estimate of the global burden of
753 anthropogenic ozone and fine particulate matter on premature human mortality using
754 atmospheric modeling, *Environ Health Perspect*, 118, 1189-1195,
755 <https://doi.org/10.1289/ehp.0901220>, 2010.

756 Baasandorj, M., Hoch, S. W., Bares, R., Lin, J. C., Brown, S. S., Millet, D. B., Martin, R., Kelly, K.,
757 Zarzana, K. J., Whiteman, C. D., Dube, W. P., Tonnesen, G., Jaramillo, I. C., and Sohl, J.:
758 Coupling between Chemical and Meteorological Processes under Persistent Cold-Air Pool
759 Conditions: Evolution of Wintertime PM_{2.5} Pollution Events and N₂O₅ Observations in Utah's
760 Salt Lake Valley, *Environ Sci Technol*, 51, 5941-5950, <https://doi.org/10.1021/acs.est.6b06603>,
761 2017.

762 Bahreini, R., Ahmadov, R., McKeen, S. A., Vu, K. T., Dingle, J. H., Apel, E. C., Blake, D. R., Blake,
763 N., Campos, T. L., Cantrell, C., Flocke, F., Fried, A., Gilman, J. B., Hills, A. J., Hornbrook, R.
764 S., Huey, G., Kaser, L., Lerner, B. M., Mauldin, R. L., Meinardi, S., Montzka, D. D., Richter,
765 D., Schroeder, J. R., Stell, M., Tanner, D., Walega, J., Weibring, P., and Weinheimer, A.:
766 Sources and characteristics of summertime organic aerosol in the Colorado Front Range:
767 perspective from measurements and WRF-Chem modeling, *Atmos. Chem. Phys.*, 18, 8293-
768 8312, <https://doi.org/10.5194/acp-18-8293-2018>, 2018.

769 Baklanov, A., Molina, L. T., and Gauss, M.: Megacities, air quality and climate, *Atmospheric*
770 *Environment*, 126, 235-249, <https://doi.org/10.1016/j.atmosenv.2015.11.059>, 2016.

771 Brauer, M., Freedman, G., Frostad, J., van Donkelaar, A., Martin, R. V., Dentener, F., van Dingenen,
772 R., Estep, K., Amini, H., Apte, J. S., Balakrishnan, K., Barregard, L., Broday, D., Feigin, V.,
773 Ghosh, S., Hopke, P. K., Knibbs, L. D., Kokubo, Y., Liu, Y., Ma, S. F., Morawska, L., Sangrador,
774 J. L. T., Shaddick, G., Anderson, H. R., Vos, T., Forouzanfar, M. H., Burnett, R. T., and Cohen,
775 A.: Ambient Air Pollution Exposure Estimation for the Global Burden of Disease 2013,
776 *Environ. Sci. Technol.*, 50, 79-88, <https://doi.org/10.1021/acs.est.5b03709>, 2016.

777 Chen, S. H. and Sun, W. Y.: A one-dimensional time dependent cloud model, *J. Meteorol. Soc. Jpn.*,
778 80, 99-118, <https://doi.org/10.2151/jmsj.80.99>, 2002.

Chen, R., Yin, P., Meng, X., Liu, C., Wang, L., Xu, X., Ross, J. A., Tse, L. A., Zhao, Z., Kan, H.,
and Zhou, M.: Fine Particulate Air Pollution and Daily Mortality. A Nationwide Analysis in
Chinese Cities, *Am J Respir Crit Care Med*, 196, 73-81,
<https://doi.org/10.1164/rccm.201609-1862OC>, 2017.

~~Crosman, E. T. and Horel, J. D.: Sea and Lake Breezes: A Review of Numerical Studies, *Boundary-Layer Meteorology*, 137, 1-29, <https://doi.org/10.1007/s10546-010-9517-9>, 2010.~~

Dai, X. A., Johnson, B. A., Luo, P. L., Yang, K., Dong, L. X., Wang, Q., Liu, C., Li, N. W., Lu, H.,
Ma, L., Yang, Z. L., and Yao, Y. Z.: Estimation of Urban Ecosystem Services Value: A Case
Study of Chengdu, Southwestern China, *Remote Sens.*, 13, 24,
<https://doi.org/10.3390/rs13020207>, 2021.

~~De Wekker S F J, Snyder B J. Mountain weather research and forecasting: recent progress and
current challenges [M]. New York: Springer, 2013.~~

Fast, J. D., Gustafson, W. I., Easter, R. C., Zaveri, R. A., Barnard, J. C., Chapman, E. G., Grell, G.
A., and Peckham, S. E.: Evolution of ozone, particulates, and aerosol direct radiative forcing
in the vicinity of Houston using a fully coupled meteorology-chemistry-aerosol model, *J.*
Geophys. Res.-Atmos., 111, 29, <https://doi.org/10.1029/2005jd006721>, 2006.

Grell, G. A. and Devenyi, D.: A generalized approach to parameterizing convection combining
ensemble and data assimilation techniques, *Geophys. Res. Lett.*, 29, 4,
<https://doi.org/10.1029/2002gl015311>, 2002.

Grell, G. A., Peckham, S. E., Schmitz, R., McKeen, S. A., Frost, G., Skamarock, W. C., and Eder,
B.: Fully coupled “online” chemistry within the WRF model, *Atmospheric Environment*, 39,
6957-6975, <https://doi.org/10.1016/j.atmosenv.2005.04.027>, 2005.

Guenther, A., Karl, T., Harley, P., Wiedinmyer, C., Palmer, P. I., and Geron, C.: Estimates of global
terrestrial isoprene emissions using MEGAN (Model of Emissions of Gases and Aerosols from
Nature), *Atmos. Chem. Phys.*, 6, 3181-3210, <https://doi.org/10.5194/acp-6-3181-2006>, 2006.

Guo, H., Ling, Z. H., Cheung, K., Jiang, F., Wang, D. W., Simpson, I. J., Barletta, B., Meinardi, S.,
Wang, T. J., Wang, X. M., Saunders, S. M., and Blake, D. R.: Characterization of
photochemical pollution at different elevations in mountainous areas in Hong Kong, *Atmos.*
Chem. Phys., 13, 3881-3898, <https://doi.org/10.5194/acp-13-3881-2013>, 2013.

Holman, C., Harrison, R. M., and Querol, X.: Review of the efficacy of low emission zones to

improve urban air quality in European cities, *Atmospheric Environment*, 111, 161-169,
<https://doi.org/10.1016/j.atmosenv.2015.04.009>, 2015.

Hu, Y. and Wang, S.: Formation mechanism of a severe air pollution event: A case study in the
 Sichuan Basin, Southwest China, *Atmospheric Environment*, 246,
<https://doi.org/10.1016/j.atmosenv.2020.118135>, 2021.

Hu, J., Li, Y. C., Zhao, T. L., Liu, J., Hu, X. M., Liu, D. Y., Jiang, Y. C., Xu, J. M., and Chang, L. Y.:
 An important mechanism of regional O₃ transport for summer smog over the Yangtze River
 Delta in eastern China, *Atmos. Chem. Phys.*, 18, 16239-16251, <https://doi.org/10.5194/acp-18-16239-2018>, 2018.

Janjic, Z. I.: THE STEP-MOUNTAIN ETA COORDINATE MODEL - FURTHER
 DEVELOPMENTS OF THE CONVECTION, VISCOUS SUBLAYER, AND
 TURBULENCE CLOSURE SCHEMES, *Mon. Weather Rev.*, 122, 927-945,
[https://doi.org/10.1175/1520-0493\(1994\)122<0927:Tsmecm>2.0.Co;2](https://doi.org/10.1175/1520-0493(1994)122<0927:Tsmecm>2.0.Co;2), 1994.

Jimenez, P. A. and Dudhia, J.: Improving the Representation of Resolved and Unresolved
 Topographic Effects on Surface Wind in the WRF Model, *J. Appl. Meteorol. Climatol.*, 51,
 300-316, <https://doi.org/10.1175/jamc-d-11-084.1>, 2012.

Jin, X. M., Fiore, A., Boersma, K. F., De Smedt, I., and Valin, L.: Inferring Changes in Summertime
 Surface Ozone-NO_x-VOC Chemistry over US Urban Areas from Two Decades of Satellite and
 Ground-Based Observations, *Environ. Sci. Technol.*, 54, 6518-6529,
<https://doi.org/10.1021/acs.est.9b07785>, 2020.

Karl, T., Gohm, A., Rotach, M. W., Ward, H. C., Graus, M., Cede, A., Wohlfahrt, G., Hammerle, A.,
 Haid, M., Tiefengraber, M., Lamprecht, C., Vergeiner, J., Kreuter, A., Wagner, J., and
 Staudinger, M.: Studying Urban Climate and Air Quality in the Alps: The Innsbruck
 Atmospheric Observatory, *Bull. Amer. Meteorol. Soc.*, 101, E488-E507,
<https://doi.org/10.1175/bams-d-19-0270.1>, 2019.

Kinney, P. L.: Interactions of Climate Change, Air Pollution, and Human Health, *Curr. Environ.
 Health Rep.*, 5, 179-186, <https://doi.org/10.1007/s40572-018-0188-x>, 2018.

Lee, C. S. L., Chou, C. C., Cheung, H. C., Tsai, C. Y., Huang, W. R., Huang, S. H., Chen, M. J.,
 Liao, H. T., Wu, C. F., Tsao, T. M., Tsai, M. J., and Su, T. C.: Seasonal variation of chemical
 characteristics of fine particulate matter at a high-elevation subtropical forest in East Asia,

839 Environ Pollut, 246, 668-677, <https://doi.org/10.1016/j.envpol.2018.11.033>, 2019.

840 Lelieveld, J., Barlas, C., Giannadaki, D., and Pozzer, A.: Model calculated global, regional and
841 megacity premature mortality due to air pollution, *Atmos. Chem. Phys.*, 13, 7023-7037,
842 <https://doi.org/10.5194/acp-13-7023-2013>, 2013.

843 Liao, J., Wang, T., Jiang, Z., Zhuang, B., Xie, M., Yin, C., Wang, X., Zhu, J., Fu, Y., and Zhang, Y.:
844 WRF/Chem modeling of the impacts of urban expansion on regional climate and air pollutants
845 in Yangtze River Delta, China, *Atmospheric Environment*, 106, 204-214,
846 <https://doi.org/10.1016/j.atmosenv.2015.01.059>, 2015.

847 Lin, B. and Zhu, J.: Changes in urban air quality during urbanization in China, *J. Clean Prod.*, 188,
848 312-321, <https://doi.org/10.1016/j.jclepro.2018.03.293>, 2018.

849 Liu, H., Liu, S., Xue, B., Lv, Z., Meng, Z., Yang, X., Xue, T., Yu, Q., and He, K.: Ground-level
850 ozone pollution and its health impacts in China, *Atmospheric Environment*, 173, 223-230,
851 <https://doi.org/10.1016/j.atmosenv.2017.11.014>, 2018.

852 Lu, H. X., Lyu, X. P., Cheng, H. R., Ling, Z. H., and Guo, H.: Overview on the spatial-temporal
853 characteristics of the ozone formation regime in China, *Environ. Sci.-Process Impacts*, 21, 916-
854 929, <https://doi.org/10.1039/c9em00098d>, 2019.

855 Luo, Y. L., Shen, J., Chen, A. F., Tao, Q., Li, Q. Q., White, P. J., Li, T. Q., Li, B., Chen, L., Li, H.
856 X., Gao, X. S., Xu, Q., and Wang, C. Q.: Loss of organic carbon in suburban soil upon
857 urbanization of Chengdu megacity, China, *Sci. Total Environ.*, 785, 10,
858 <https://doi.org/10.1016/j.scitotenv.2021.147209>, 2021.

859 Manisalidis, I., Stavropoulou, E., Stavropoulos, A., and Bezirtzoglou, E.: Environmental and Health
860 Impacts of Air Pollution: A Review, *Frontiers in Public Health*, 8,
861 <https://doi.org/10.3389/fpubh.2020.00014>, 2020.

862 Matsui, T., Zhang, S. Q., Lang, S. E., Tao, W. K., Ichoku, C., and Peters-Lidard, C. D.: Impact of
863 radiation frequency, precipitation radiative forcing, and radiation column aggregation on
864 convection-permitting West African monsoon simulations, *Clim. Dyn.*, 55, 193-213,
865 <https://doi.org/10.1007/s00382-018-4187-2>, 2018.

866 Mlawer, E. J., Taubman, S. J., Brown, P. D., Iacono, M. J., and Clough, S. A.: Radiative transfer for
867 inhomogeneous atmospheres: RRTM, a validated correlated-k model for the longwave, *J.*
868 *Geophys. Res.-Atmos.*, 102, 16663-16682, <https://doi.org/10.1029/97jd00237>, 1997.

Molina, L. T., Madronich, S., Gaffney, J. S., Apel, E., de Foy, B., Fast, J., Ferrare, R., Herndon, S., Jimenez, J. L., Lamb, B., Osornio-Vargas, A. R., Russell, P., Schauer, J. J., Stevens, P. S., Volkamer, R., and Zavala, M.: An overview of the MILAGRO 2006 Campaign: Mexico City emissions and their transport and transformation, *Atmos. Chem. Phys.*, 10, 8697-8760, <https://doi.org/10.5194/acp-10-8697-2010>, 2010.

Ning, G., Wang, S., Yim, S. H. L., Li, J., Hu, Y., Shang, Z., Wang, J., and Wang, J.: Impact of low-pressure systems on winter heavy air pollution in the northwest Sichuan Basin, China, *Atmos. Chem. Phys.*, 18, 13601-13615, <https://doi.org/10.5194/acp-18-13601-2018>, 2018.

~~Oke, T. R.; Mills, G.; Christen, A.; Voogt, J. A. Urban Climates; Cambridge University Press; Cambridge, 2017.~~

Pautasso, M., Dehnen-Schmutz, K., Holdenrieder, O., Pietravalle, S., Salama, N., Jeger, M. J., Lange, E., and Hehl-Lange, S.: Plant health and global change - some implications for landscape management, *Biol. Rev.*, 85, 729-755, <https://doi.org/10.1111/j.1469-185X.2010.00123.x>, 2010.

Qian, Y., Chakraborty, T. C., Li, J., Li, D., He, C., Sarangi, C., Chen, F., Yang, X., and Leung, L. R.: Urbanization Impact on Regional Climate and Extreme Weather: Current Understanding, Uncertainties, and Future Research Directions, *Adv Atmos Sci*, 1-42, <https://doi.org/10.1007/s00376-021-1371-9>, 2022.

Ryu, Y. H., Baik, J. J., Kwak, K. H., Kim, S., and Moon, N.: Impacts of urban land-surface forcing on ozone air quality in the Seoul metropolitan area, *Atmos. Chem. Phys.*, 13, 2177-2194, <https://doi.org/10.5194/acp-13-2177-2013>, 2013.

Schell, B., Ackermann, I. J., Hass, H., Binkowski, F. S., and Ebel, A.: Modeling the formation of secondary organic aerosol within a comprehensive air quality model system, *J. Geophys. Res.-Atmos.*, 106, 28275-28293, <https://doi.org/10.1029/2001jd000384>, 2001.

Seto, K. C., Guneralp, B., and Hutyrá, L. R.: Global forecasts of urban expansion to 2030 and direct impacts on biodiversity and carbon pools, *Proc. Natl. Acad. Sci. U. S. A.*, 109, 16083-16088, <https://doi.org/10.1073/pnas.1211658109>, 2012.

Shu, Z., Liu, Y., Zhao, T., Xia, J., Wang, C., Cao, L., Wang, H., Zhang, L., Zheng, Y., Shen, L., Luo, L., and Li, Y.: Elevated 3D structures of PM_{2.5} and impact of complex terrain-forcing circulations on heavy haze pollution over Sichuan Basin, China, *Atmos. Chem. Phys.*, 21,

9253-9268, <https://doi.org/10.5194/acp-21-9253-2021>, 2021.

Song, Y., Wang, X., Maher, B. A., Li, F., Xu, C., Liu, X., Sun, X., and Zhang, Z.: The spatial-temporal characteristics and health impacts of ambient fine particulate matter in China, *J. Clean Prod.*, 112, 1312-1318, <https://doi.org/10.1016/j.jclepro.2015.05.006>, 2015.

Stockwell, W. R., Middleton, P., Chang, J. S., and Tang, X. Y.: THE 2ND GENERATION REGIONAL ACID DEPOSITION MODEL CHEMICAL MECHANISM FOR REGIONAL AIR-QUALITY MODELING, *J. Geophys. Res.-Atmos.*, 95, 16343-16367, <https://doi.org/10.1029/JD095iD10p16343>, 1990.

Tang, G. Q., Zhu, X. W., Xin, J. Y., Hu, B., Song, T., Sun, Y., Zhang, J. Q., Wang, L. L., Cheng, M. T., Chao, N., Kong, L. B., Li, X., and Wang, Y. S.: Modelling study of boundary-layer ozone over northern China - Part I: Ozone budget in summer, *Atmos. Res.*, 187, 128-137, <https://doi.org/10.1016/j.atmosres.2016.10.017>, 2017.

Tewari, M., Chen, F., Wang, W., Dudhia, J., LeMone, M., Mitchell, K., Ek, M., Gayno, G., Wegiel, J., and Cuenca, R.: Implementation and verification of the unified NOAH land surface model in the WRF model, 20th conference on weather analysis and forecasting/16th conference on numerical weather prediction, 2165-2170.

UN DESA, 2018: World Urbanization Prospects: The 2018 Revision. United Nations Department of Economic and Social Affairs, Population Division.

Wang, H., Liu, Z., Wu, K., Qiu, J., Zhang, Y., Ye, B., and He, M.: Impact of Urbanization on Meteorology and Air Quality in Chengdu, a Basin City of Southwestern China, *Frontiers in Ecology and Evolution*, 10, <https://doi.org/10.3389/fevo.2022.845801>, 2022a.

Wang, H., Liu, Z., Zhang, Y., Yu, Z., and Chen, C.: Impact of different urban canopy models on air quality simulation in Chengdu, southwestern China, *Atmospheric Environment*, 267, <https://doi.org/10.1016/j.atmosenv.2021.118775>, 2021.

~~Wang, P., Shen, J., Xia, M., Sun, S., Zhang, Y., Zhang, H., and Wang, X.: Unexpected enhancement of ozone exposure and health risks during National Day in China, *Atmos. Chem. Phys.*, 21, 10347-10356, <https://doi.org/10.5194/acp-21-10347-2021>, 2021.~~ Wang, X., Chen, F., Wu, Z., Zhang, M., Tewari, M., Guenther, A., and Wiedinmyer, C.: Impacts of weather conditions modified by urban expansion on surface ozone: Comparison between the Pearl River Delta and Yangtze River Delta regions, *Advances in Atmospheric Sciences*, 26, 962-972, 2009.

Wang, Y., Yang, X., Wu, K., Mei, H., De Smedt, I., Wang, S., Fan, J., Lyu, S., and He, C.: Long-term trends of ozone and precursors from 2013 to 2020 in a megacity (Chengdu), China: Evidence of changing emissions and chemistry, *Atmos. Res.*, 278, <https://doi.org/10.1016/j.atmosres.2022.106309>, 2022b.

Whiteman C D. Mountain meteorology: fundamentals and applications [M]. Oxford University Press, 2000.

Wu, K., Wang, Y., Qiao, Y., Liu, Y., Wang, S., Yang, X., Wang, H., Lu, Y., Zhang, X., and Lei, Y.: Drivers of 2013-2020 ozone trends in the Sichuan Basin, China: Impacts of meteorology and precursor emission changes, *Environ Pollut*, 300, 118914, <https://doi.org/10.1016/j.envpol.2022.118914>, 2022.

Yang, X., Wu, K., Wang, H., Liu, Y., Gu, S., Lu, Y., Zhang, X., Hu, Y., Ou, Y., Wang, S., and Wang, Z.: Summertime ozone pollution in Sichuan Basin, China: Meteorological conditions, sources and process analysis, *Atmospheric Environment*, 226, <https://doi.org/10.1016/j.atmosenv.2020.117392>, 2020.

Yin, P., Chen, R., Wang, L., Meng, X., Liu, C., Niu, Y., Lin, Z., Liu, Y., Liu, J., Qi, J., You, J., Zhou, M., and Kan, H.: Ambient Ozone Pollution and Daily Mortality: A Nationwide Study in 272 Chinese Cities, *Environ Health Perspect*, 125, 117006, <https://doi.org/10.1289/EHP1849>, 2017.

Yu, M., Carmichael, G. R., Zhu, T., and Cheng, Y.: Sensitivity of predicted pollutant levels to urbanization in China, *Atmospheric Environment*, 60, 544-554, <https://doi.org/10.1016/j.atmosenv.2012.06.075>, 2012.

Zardi, D. and Whiteman, C. D.: Diurnal Mountain Wind Systems, in *Mountain weather research and forecasting*, edited by: Chow, F. K., De Wekker, S. F. J., and Snyder, B., Springer, Berlin, 2013.

Zhan, C. and Xie, M.: Land use and anthropogenic heat modulate ozone by meteorology: a perspective from the Yangtze River Delta region, *Atmos. Chem. Phys.*, 22, 1351-1371, <https://doi.org/10.5194/acp-22-1351-2022>, 2022.

Zhan, C., Xie, M., Liu, J., Wang, T., Xu, M., Chen, B., Li, S., Zhuang, B., and Li, M.: Surface Ozone in the Yangtze River Delta, China: A Synthesis of Basic Features, Meteorological Driving Factors, and Health Impacts, *Journal of Geophysical Research: Atmospheres*, 126, <https://doi.org/10.1029/2020jd033600>, 2021.

959 Zhan, C.-c., Xie, M., Fang, D.-x., Wang, T.-j., Wu, Z., Lu, H., Li, M.-m., Chen, P.-l., Zhuang, B.-l.,
960 Li, S., Zhang, Z.-q., Gao, D., Ren, J.-y., and Zhao, M.: Synoptic weather patterns and their
961 impacts on regional particle pollution in the city cluster of the Sichuan Basin, China,
962 Atmospheric Environment, 208, 34-47, <https://doi.org/10.1016/j.atmosenv.2019.03.033>, 2019.
963 Zhu, K. G., Xie, M., Wang, T. J., Cai, J. X., Li, S. B., and Feng, W.: A modeling study on the effect
964 of urban land surface forcing to regional meteorology and air quality over South China,
965 Atmospheric Environment, 152, 389-404, <https://doi.org/10.1016/j.atmosenv.2016.12.053>,
966 2017.